Sensor and Simulation Notes

Note 235

12 December 1977

AN ANALYTICAL INVESTIGATION OF THE METHOD OF USING AN EXTRAPOLATION FUNCTION IN FINDING CRITERIA RESPONSE FROM SIMULATION RESPONSE

Kuan Min Lee
Mission Research Corporation
Albuquerque, New Mexico 87108

Abstract

The extrapolation techniques outlined in Sensor and Simulation Note 222 are discussed. The methods are applied to an infinite cylinder problem as well as a finite cylinder problem using theoretical models. The effects of the angle of incidence is also examined using the infinite cylinder model. Some conclusions about the utility of the methods in error estimations are drawn based on these analytical investigations.

TABLE OF CONTENTS

LIST OF ILLUSTRATIONS

LIST OF ILLUSTRATIONS (continued)

LIST OF ILLUSTRATIONS (continued)

SECTION I

AN INVESTIGATION OF THE METHOD OF USING EXTRAPOLATION FUNCTION IN FINDING CRITERIA RESPONSE FROM SIMULATION RESPONSE

1.1 INTRODUCTION

In the analysis of the electromagnetic field problems, it is often necessary to use the principle of electrodynamic similitude in the design of apparatus. It has been shown using Maxwell's equations that, in order that two electromagnetic boundary-value problems be similar, it is necessary and sufficient that certain coefficients be identical in both (ref. 1). This has always been the guide line for designing experiments. However, suppose that the true or criteria environment is so difficult to construct so that the simulation environment is not quite similar to the criteria environment, what is the remedy to extrapolate useful information from the simulation response? In particular, consider the problem of finding the EMP response in an electronic circuit inside an airplane in free space due to a nuclear burst (Fig. 1a). Instead of simulating the awkward true situation, measurements were made in an airplane near ground with a pulse generator as shown in Figure 1b. Is it possible to find the criteria response from the measured simulation response inside the airplane if the scattered fields outside the airplane are given but the transfer functions between these fields outside and the response inside are not known? It has been proposed recently that this problem could be solved by making use of certain "extrapolation functions" if some error bounds in the result were allowed (ref. 2).

It is the purpose of this study to investigate this proposal by applying the suggested method to a typical problem.

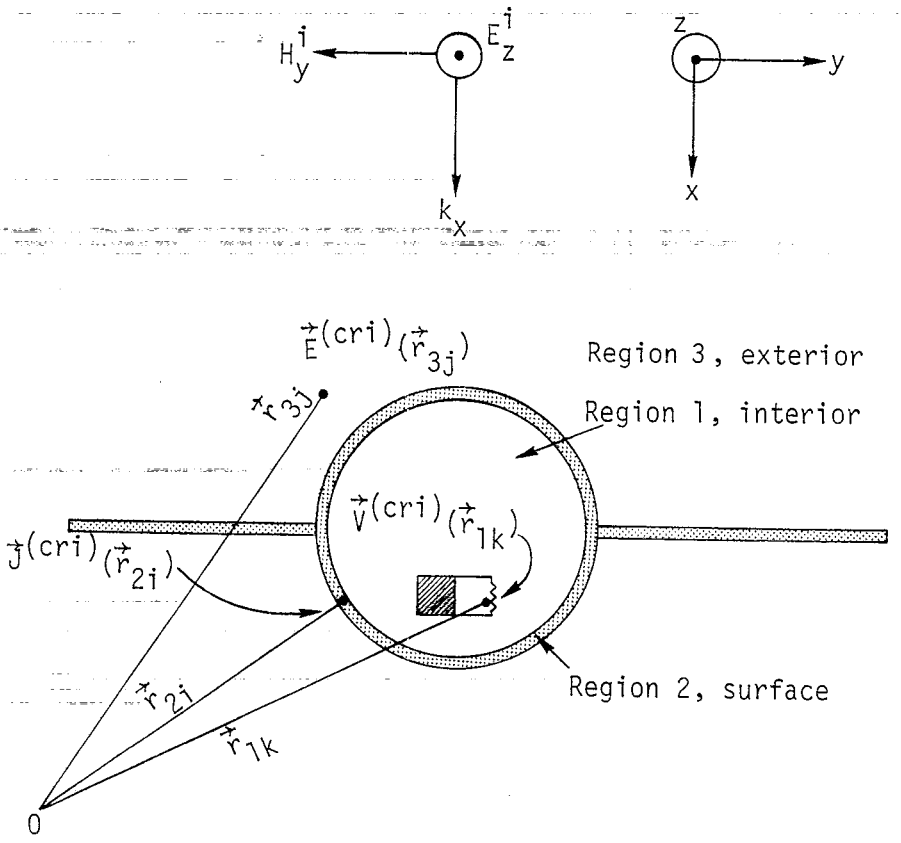

Figure 1a. Airplane in Free Space.

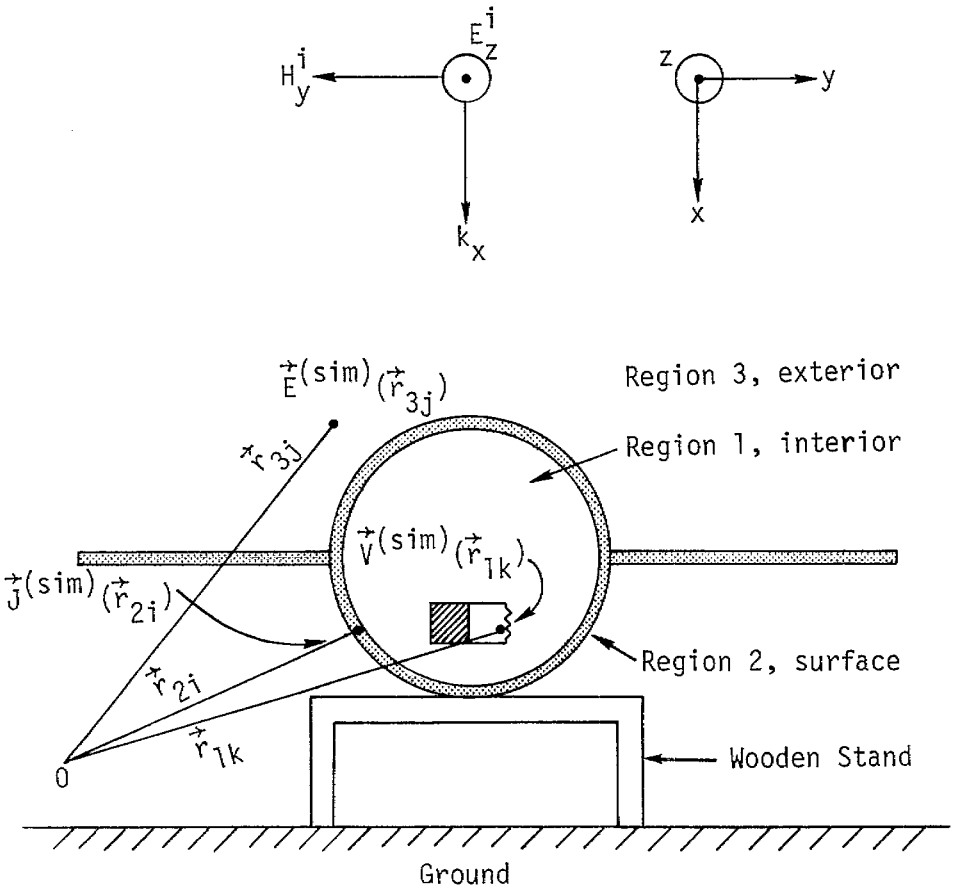

Figure 1b. Airplane Near Ground.

1.2 NOTATIONS AND DEFINITIONS (ref. 2)

Some notations and definitions used in this report will be summarized briefly in this section. Consider the example in Figures 1a and 1b again. Let the space be divided into three regions where region 1 is the interior region inside the airplane with position vector $\vec{r}_1$, region 2 is the aircraft surface region with the position vector $\vec{r}_2$, and region 3 is the space exterior to the aircraft with the position vector $\vec{r}_3$. The voltage response measured in the k^{th} circuit component in region 1 will be called $V(\vec{r}_{1k})$. The current measured at the i^{th} location of the aircraft surface (region 2) will be called $\vec{J}(\vec{r}_{2i})$. The electric field measured at j^{th} location in region 3 will be called $\vec{E}(\vec{r}_{3j})$. In order to distinguish the criteria situation from the simulation situation, we associate the superscript "sim" with the quantities in the simulation environment and "cri" with the quantities in the criteria environment. Thus, for a measured voltage on the k^{th} circuit in region 1, in the criteria environment, the notation is $V^{(cri)}(\vec{r}_{1k})$.

The field in region 1 is induced by the electromagnetic fields in regions 2 and 3 through the port of entry. They are related by the transfer functions $T(\vec{r}_{2i},\vec{r}_{1k})$, etc. The transfer functions relating fields between regions 2 and 3 can be determined by solving the exterior problem (refs. 3 and 4) and will not be discussed in this report.

Therefore, all the transfer functions considered here will be those between region 1 and region 2 with the first position vector referring to those in region 2 and the second position vector referring to those in region 1. Note that the transfer functions are varied with frequencies as well as positions. Thus, for measured quantities $V^{(sim)}(\vec{r}_{1k})$ and $\vec{J}^{(sim)}(\vec{r}_{2i})$ in the frequency domain, we have

$$V^{(sim)}(\vec{r}_{1k},\omega) = \sum_{i=1}^{N} T^{(sim)}(\vec{r}_{2i}, \vec{r}_{1k}, \omega)\, J^{(sim)}(\vec{r}_{2i}, \omega) \quad . \quad (1)$$

If we restrict the discussion of the transfer functions to those between region 1 and 2, and note that the left hand member in equation (1) is always in region 1, whereas the right hand response (in this case, $J^{(sim)}$) is always in region 2, we may simplify the notations by dropping the superscript and write equation (1) as

$$V_k^{(sim)}(\omega) = \sum_{i=1}^{N} T_{ik}^{(sim)}(\omega)\ J_i^{(sim)}(\omega) \qquad (2)$$

where i and k are simplified notations for $\vec{r}_i$ and $\vec{r}_k$.

An equation similar to (2) can be written down for the criteria situation,

$$V_k^{(cri)}(\omega) = \sum_{i=1}^{N} T_{ik}^{(cri)}(\omega)\ J_i^{(cri)}(\omega) \qquad . \quad (3)$$

We now make an assumption that the transfer functions in equations (2) and (3) are the same so that

$$T_{ik}^{(sim)}(\omega) = T_{ik}^{(cri)}(\omega) = T_{ik}(\omega) \qquad . \quad (4)$$

This assumption will be reasonable if the interior configuration as well as the surface configuration remains unchanged in the criteria environment and the simulation environment. Using equation (4) in equations (2) and (3) we have

$$V_k^{(sim)}(\omega) = \sum_{i=1}^{N} T_{ik}(\omega)\ J_i^{(sim)}(\omega) \qquad (5)$$

$$V_k^{(cri)}(\omega) = \sum_{i=1}^{N} T_{ik}(\omega)\ J_i^{(cri)}(\omega) \qquad . \quad (6)$$

The quantities $J_i^{(sim)}(\omega)$ and $J_i^{(cri)}(\omega)$ can be calculated or measured from the exterior problem. The quantity $V_k^{(sim)}(\omega)$ can be measured, and $V^{(cri)}(\omega)$ is the unknown quantity that we are seeking. If the values of $T_{ik}(\omega)$ are given, the problem can be easily solved. Difficulties arise in a real situation where the point of entry and the transfer function is not known.

In order to circumvent this difficulty, a quantity called "extrapolation function" $R_i(\omega)$ is introduced, where

$$R_i(\omega) = \frac{J_i^{(cri)}(\omega)}{J_i^{(sim)}(\omega)} \quad . \quad (7)$$

Using this definition, equation (6) becomes,

$$V_k^{(cri)}(\omega) = \sum_{i=1}^{N} T_{ik}(\omega)\, J_i^{(sim)}(\omega)\, R_i(\omega) \quad . \quad (8)$$

In general, $R_i(\omega)$ is a function of both frequency and the position and is not a constant.

If there is only one port of entry, equation (8) reduces to

$$V_k^{(cri)}(\omega) = T_{ik}(\omega)\, J_i^{(sim)}(\omega)\, R_i(\omega) \quad (9)$$

and from equation (5)

$$V_k^{(sim)}(\omega) = T_{ik}(\omega)\, J_i^{(sim)}(\omega) \quad (10)$$

so that

$$V_k^{(cri)}(\omega) = V_k^{(sim)}(\omega)\, R_i(\omega) \quad (11)$$

and $V_k^{(cri)}(\omega)$ can be determined.

Another special case is when $R_i(\omega) \equiv C$ a constant, then equation (8) becomes,

$$V_k^{(cri)}(\omega) = C\sum_{i=1}^{N} T_{ik}(\omega)\, J_i^{(sim)}(\omega) = C\, V_k^{(sim)}(\omega) \quad . \quad (12)$$

In particular, when $C = 1$, the two problems are entirely similar. It is easy to see from equation (12) that, if $R_i(\omega)$ is a constant, the criteria response $V_k^{(cri)}(\omega)$ can be derived from the simulation response in a simple manner. In general, if some constant (say, a number obtained by taking the average of $R_i(\omega)$ over all positions i) is used in replacing each individual $R_i(\omega)$, it will result in some error since $R_i(\omega)$ is not a constant under most circumstances. However, due to the simplicity of equation (12), it is interesting to study the above procedure and the possible error bounds more colsely. The error can be obtained roughly by examining the ratio $R_i(\omega)/F(\omega)$ as a function of frequency, where $F(\omega)$ is a selected testing function which is not a function of positions. In this study, we shall select the following test function:

$$F1(\omega) = EXP\left(\frac{1}{N}\sum_{i=1}^{N} \log_e R_i(\omega)\right) \quad . \quad (13)$$

1.3 A TYPICAL PROBLEM

Consider the problem of an infinite cylindrical conductor in the presence of an incident plane wave with and without a ground plane as shown in Figures 2a and 2b. Let the electric field component of the incident plane wave be parallel to the axis of the cylinder, with the wave propagating along positive x direction.

The coordinate systems are as shown in Figures 2a and 2b. Then, the incident electric field can be written as

$$E_z^i = E_0\, e^{-jkx}\, e^{+j\omega t} \quad . \quad (14)$$

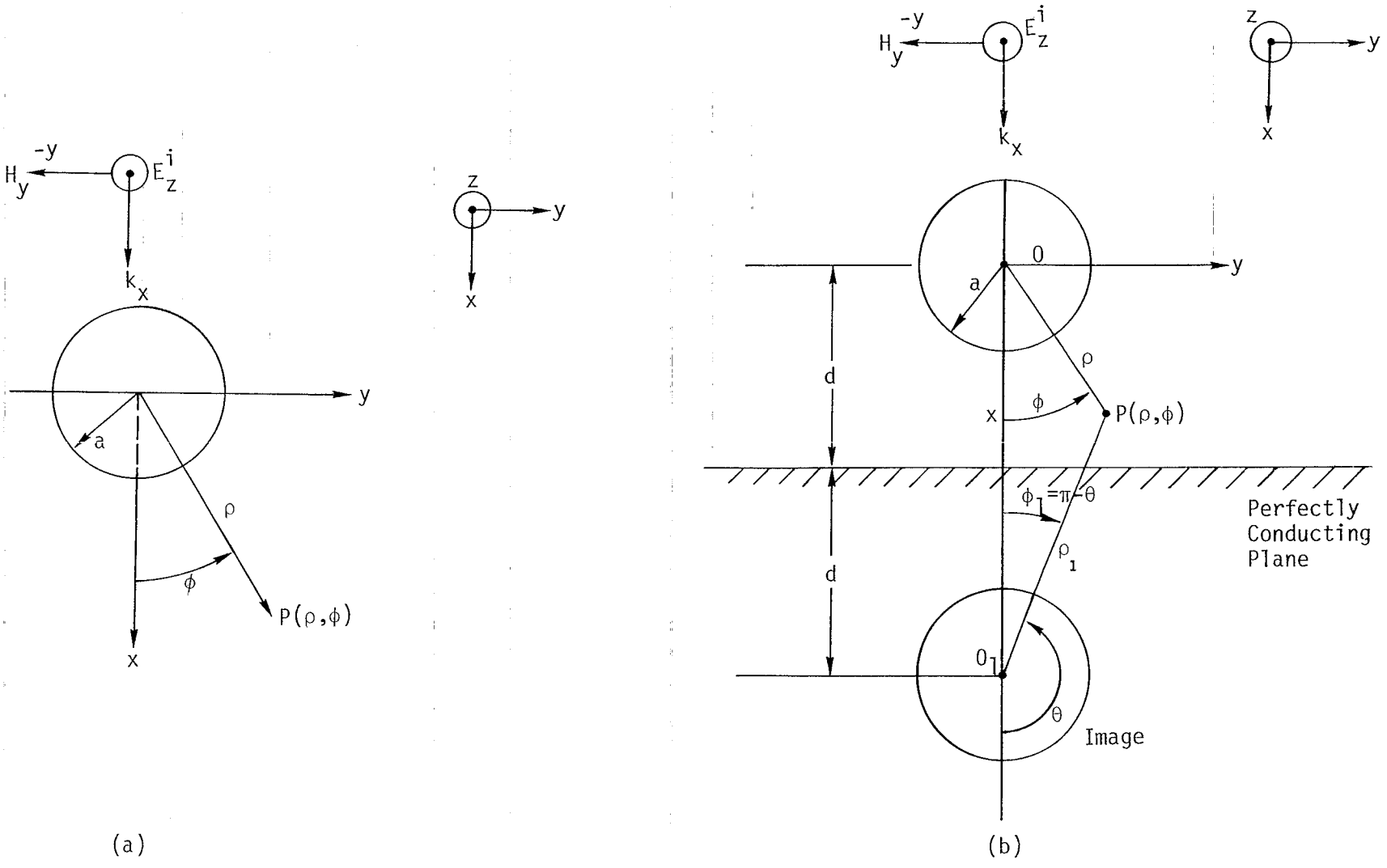

Figure 2. An infinite cylindrical conductor in the presence of an incident plane wave, (a) without a ground plane and (b) with a ground plane.

To solve the problem shown in Figure 2a, equation (14) can be expanded in the following form (refs. 1 and 5) with $e^{+j\omega t}$ suppressed,

$$E_z^i = E_o \sum_{-\infty}^{\infty} j^{-n} J_n(k\rho)\, e^{jn\phi} \quad . \quad (15)$$

The scattered field can be assumed to be

$$E_z^s = E_o \sum_{n=-\infty}^{\infty} j^{-n} a_n H_n^{(2)}(k\rho)\, e^{jn\phi} \quad (16)$$

where $J_n(k\rho)$ is the Bessel's function of order n, and $H_n^{(2)}(k\rho)$ is the Hankel's function of the second kind with order n. At $\rho = a$, the total field $E_z^t = E_z^i + E_z^s = 0$, hence

$$a_n = - \frac{J_n(ka)}{H_n^{(2)}(ka)} \quad . \quad (17)$$

Using equations (17), (16) and (15), the total electric field can be determined. The total magnetic field is given by

$$H_\phi = \frac{1}{j\omega\mu} \frac{\partial E_z^t}{\partial \rho} \quad . \quad (18)$$

The current density on the cylinder is related to equation (18) by $J_z = H_\phi |$ at $\rho = a$. Combining the above results, it is easily found that (refs. 5 and 6)

$$J_z = \frac{2E_o}{\omega\mu\pi a} \sum_{n=-\infty}^{\infty} j^{-n} \frac{e^{jn\phi}}{H_n^{(2)}(ka)} \quad . \quad (19)$$

To solve the problem shown in Figure 2b, it is necessary to assume two more scattered fields due to the presence of the perfect conducting ground plane. Thus we have (let $R_1 = -1$)

$$E_z^i = E_o \sum_{n=-\infty}^{\infty} j^{-n} J_n(k\rho)\, e^{jn\phi} \tag{20a}$$

$$E_z^r = R_1 E_o \sum_{n=-\infty}^{\infty} j^{n} e^{-j2kd} J_n(k\rho)\, e^{-jn\phi} \tag{20b}$$

$$E_z^s = E_o \sum_{n=-\infty}^{\infty} j^{-n} a_n H_n^{(2)}(k\rho)\, e^{jn\phi} \tag{20c}$$

$$E_z^{sr} = R_1 E_o \sum_{n=-\infty}^{\infty} j^{-n} a_n H_n^{(2)}(k\rho_1)\, e^{jn\phi_1} \tag{20d}$$

$$E_z^t = E_z^i + E_z^r + E_z^s + E_z^{sr} \tag{20e}$$

where E_z^i is the incident field, E_z^r is the reflected field due to the ground plane, E_z^s is the scattered field due to the cylinder, E_z^{sr} is the scattered field due to the image of the cylinder and E_z^t is the total field. The origin O is taken to be the center of the cylinder and the ground plane is located at a distance d away from the origin. The coordinates ρ, ϕ, ρ_1 and ϕ_1, θ are as shown in Figure 2b. To show that the boundary conditions can be satisfied by these fields, note that equations (20a) and (20b) can be written as (refs. 1 and 5)

$$E_z^i = E_o\, e^{-j\, k\rho \cos\phi} = E_o e^{-jkx} \tag{21a}$$

$$E_z^r = R_1 E_o\, e^{-j2kd}\, e^{+jkx} \tag{21b}$$

For $R_1 = -1$ and $X = +d$, these lead to $E_z^i + E_z^r = 0$. Furthermore, for points on the ground plane, $\phi = \phi_1$ and $\rho = \rho_1$ so that $E_z^s + E_z^{sr} = 0$ from equation (20c) and (20d). Hence, the boundary condition on the ground plane is satisfied.

The second boundary condition is $E_z^i + E_z^r + E_z^s + E_z^{sr} = 0$ at $\rho = a$. To show this, it is convenient to express all fields in terms of the variable ρ and ϕ. This can be done by expanding equation (20d) in a different form using the addition theorem of Bessel's function (ref. 1). Referring to Figure 3, the additional theorem gives.

$$H_n^{(2)}(kr_1)\, e^{-in\theta_1} = \sum_{m=-\infty}^{\infty} H_m^{(2)}(kr_o)\, J_{m+n}(kr)\, e^{-im(\theta-\theta_o)} - in\theta \quad .(22)$$

In our case, $\theta_o = 0$, $r_o = 2kd$, $r_1 = \rho_1$, $r = \rho$, $\theta = \phi$, $\theta_1 = \pi - \phi_1$ (see Figures 2b and 3), from (20d) we have,

$$E_z^{sr} = R_1\, E_o \sum_{n=-\infty}^{\infty} j^{-n}\, a_n\, H_n^{(2)}(k\rho_1)\, e^{jn(\pi-\theta_1)}$$

$$= R_1\, E_o \sum_{n=-\infty}^{\infty} j^{+n}\, a_n \sum_{m=-\infty}^{\infty} H_m^{(2)}(2kd)\, J_{n+m}(k\rho)\, e^{-jn\phi-jm\phi} \quad . \quad (23)$$

Applying the boundary condition at $\rho = a$,

$$\sum_{n=-\infty}^{\infty} j^{-n}\, J_n(ka)\, e^{jn\phi} + \sum_{n=-\infty}^{\infty} R_1\, e^{-j2kd}\, j^n\, J_n(ka)\, e^{jn\phi}$$

$$+ \sum_{n=-\infty}^{\infty} j^{-n}\, a_n\, H_n^{(2)}(ka)\, e^{jn\phi} + \sum_{n=-\infty}^{\infty} R_1 j^n a_n \sum_{m=-\infty}^{\infty} H_m^{(2)}(2kd)\, J_{n+m}(ka)\, e^{-jn\phi-jm\phi} = 0$$

$$. \quad (24)$$

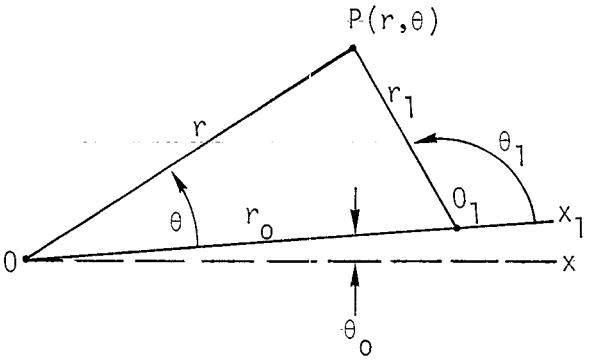

Figure 3. Coordinate for Using Additional Theorem.

Equation (24) determines the proper coefficients a_n for this problem. If we change the index in the last summation in (24), and collecting terms associated with $e^{jn\phi}$, we have

$$j^{-n} a_n H_n^{(2)}(ka) + R_1 j^{-n} a_{-n} H_o^{(2)}(2kd) J_{-n}(ka)$$

$$+ \sum_{m=1}^{\infty} R_1 j^{-(n+m)} a_{-(n+m)} H_m^{(2)}(2kd) J_{-n}(ka) + \sum_{m=1}^{\infty} R_1 j^{m-n} a_{m-n} H_m^{(2)}(2kd)(-1)^{m-n} J_n(ka)$$

$$= -(j^{-n} + R_1 e^{-j2kd} j^n) J_n(ka), \quad n = -\infty, \ldots, 0, \ldots, +\infty \qquad . \quad (25)$$

This is a matrix equation with infinite elements. A complete determination of a_n from (25) is difficult. Various approximations can be used in solving (25) depending on the accuracy of the result we are seeking. We shall consider the following approximations:

(1) A first approximation is to neglect the effects due to the scattered field of the image cylinder so that the terms with $H_m^{(2)}(2kd)\, J_n(ka)$ in equation (25) can be omitted. This leads to

$$a_n = \frac{(j^{-n} + R_1 e^{-j2kd} j^n)}{j^{-n} H_n^{(2)}(ka)} J_n(ka) \qquad (26)$$

(2) The next simple case is to use the diagonal element in the matrix in solving equation (25) (ref. 7)

$$a_n \doteq - \frac{(j^{-n} + R_1 e^{-j2kd} j^n) J_n(ka)}{j^{-n}[H_n^{(2)}(ka) + R_1 H_{2n}^{(2)}(2kd) J_n(ka)]} \qquad (27)$$

This reduces to equation (26) when $H_{2n}^{(2)}(2kd)\, J_n(ka)$ is neglected.

(3) If great accuracy is desired, it is possible to solve equation (25) for N finite modes.

For the present purpose, approximations (1) and (2) are sufficient. The current density is given as follows:

(1) Using equations (26), (20) and (18),

$$J_z = H_\phi\Big|_{\rho=a} = \frac{1}{j\omega\mu} \left.\frac{\partial E_z^t}{\partial \rho}\right|_{\rho=a}$$

$$= \frac{2E_o}{\omega\mu\pi a} \sum_{n=-\infty}^{\infty} \frac{(j^{-n} + R_1\, e^{-j2kd} j^n)}{H_n^{(2)}(ka)} \qquad (28)$$

(2) Using equations (27), (20) and (18)

$$J_z = \frac{-j\ E_o}{c\mu_o} \sum_{n=-\infty}^{\infty} j^{-n}\, J_n'(ka)\, e^{jn\phi} +$$

$$\frac{-j\ E_o}{c\mu_o} \sum_{n=-\infty}^{\infty} R_1\, e^{-j2kd}\, j^n\, J_n'(ka)\, e^{jn\phi} +$$

$$\frac{-j\ E_o}{c\mu_o} \sum_{n=-\infty}^{\infty} j^{-n}\, a_n\, H_n^{(2)'}(ka)\, e^{jn\phi} +$$

$$\frac{-j\ E_o}{c\mu_o} \sum_{n=-\infty}^{\infty} R_1\, j^n\, a_n \sum_{m=-\infty}^{\infty} H_m^{(2)}(2kd)\, J_{n+m}'(ka)\, e^{-j(m+n)\phi} \qquad (29)$$

In fact, Equation (29) is the general solution to this problem if the correct a_n's are used. In the next section, we shall discuss the application of extrapolation functions using the results derived in this section.

1.4 APPLICATION OF THE EXTRAPOLATION FUNCTION TO THE ABOVE PROBLEM

To apply the extrapolation function concept to the above problem, we make use of Equations (19) and (29) (or Eq. (28)), and derive the following function from them

$$R_i(\omega) = \frac{J_z^{(FF)}(\phi_i,\omega)}{J_z^{(HPD)}(\phi_i,\omega)} \tag{30}$$

where $J_z^{(FF)}(\phi_i,\omega)$ is used to denote the current density obtained for Figure 2a (Eq. (19)), and $J_z^{(HPD)}(\phi_i,\omega)$ is used to denote the current density obtained for Figure 2b (Eqs. (28) or (29)). Next, the average function $F1(\omega)$ is formulated according to Equation (13), that is,

$$F1(\omega) = \sqrt[N]{R_1(\omega)R_2(\omega)R_3(\omega) \ldots R_N(\omega)}, \tag{31}$$

Then, the following ratio is calculated and plotted as a function of frequency,

$$Q1_i(\omega) = \frac{R_i(\omega)}{F1(\omega)} \tag{32}$$

In Figure 4, the absolute value of $J_z^{(FF)}$ and $J_z^{(HPD)}$ is plotted as a function of frequency with angle ϕ as parameters. Figure 4a is obtained using equation (19), Figure 4b is obtained using equation (28), and Figure 4c is obtained using equation (29). Note that, at low frequency range, the current density $J_z^{(HPD)}$ is not uniform whereas $J_z^{(FF)}$ is nearly uniform.

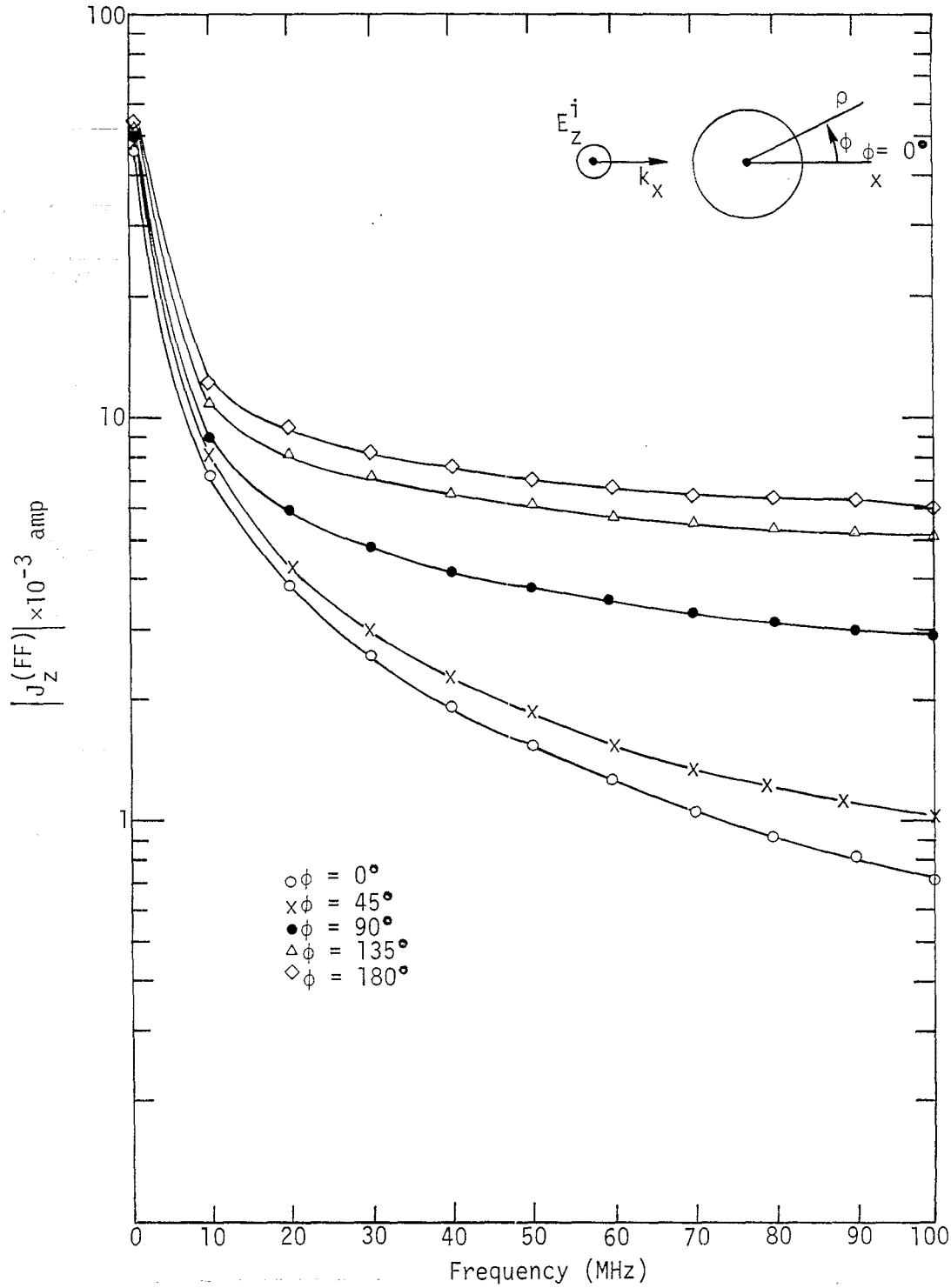

Figure 4a. $|J_z^{(FF)}|$ as a function of frequency at different angle ϕ for a cylinder with radius a = 0.5 m.

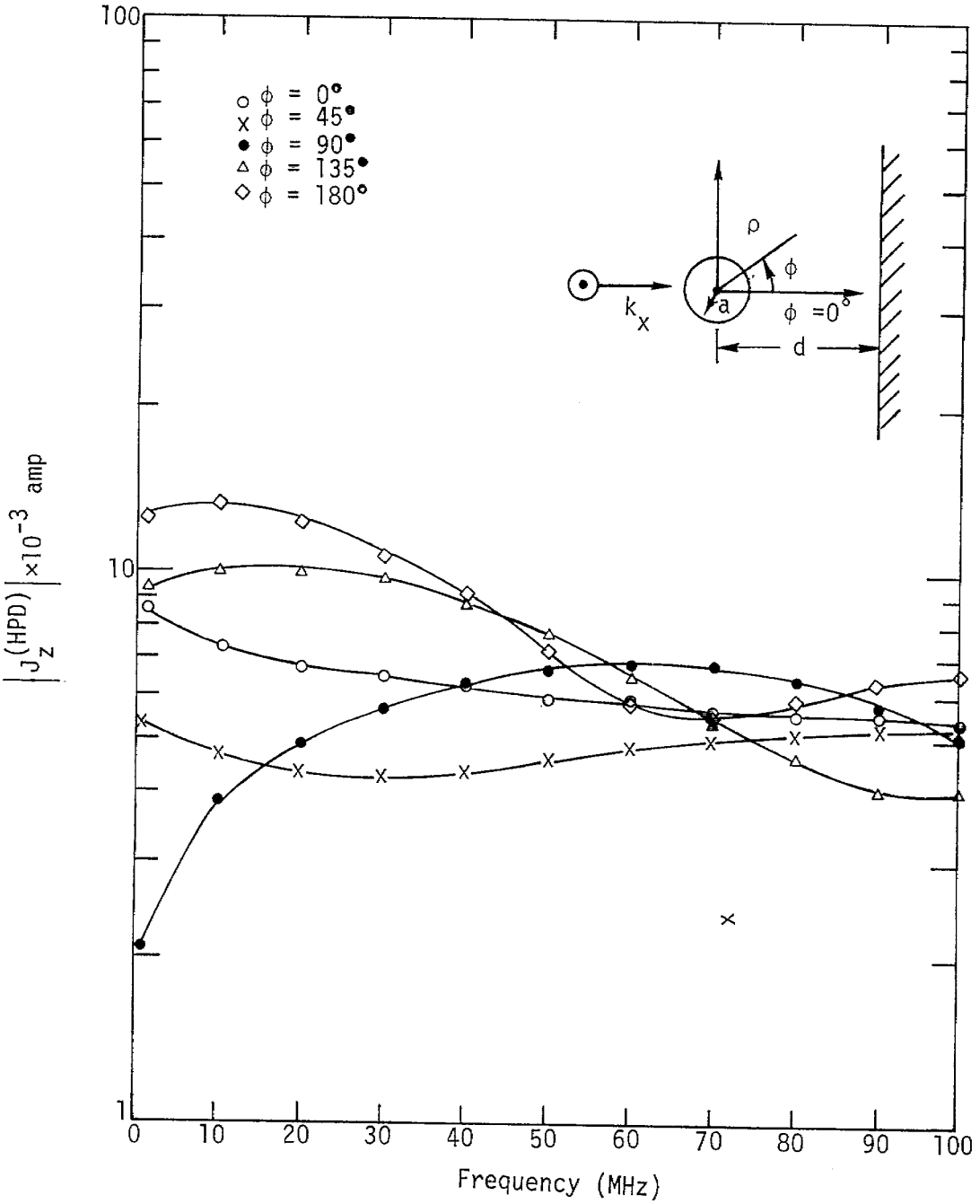

Figure 4b. $\left|J_z^{(HPD)}\right|$ as a function of frequency at different angle ϕ for a cylinder with a = 0.5 m, d = 1 m, calculated using first approximation.

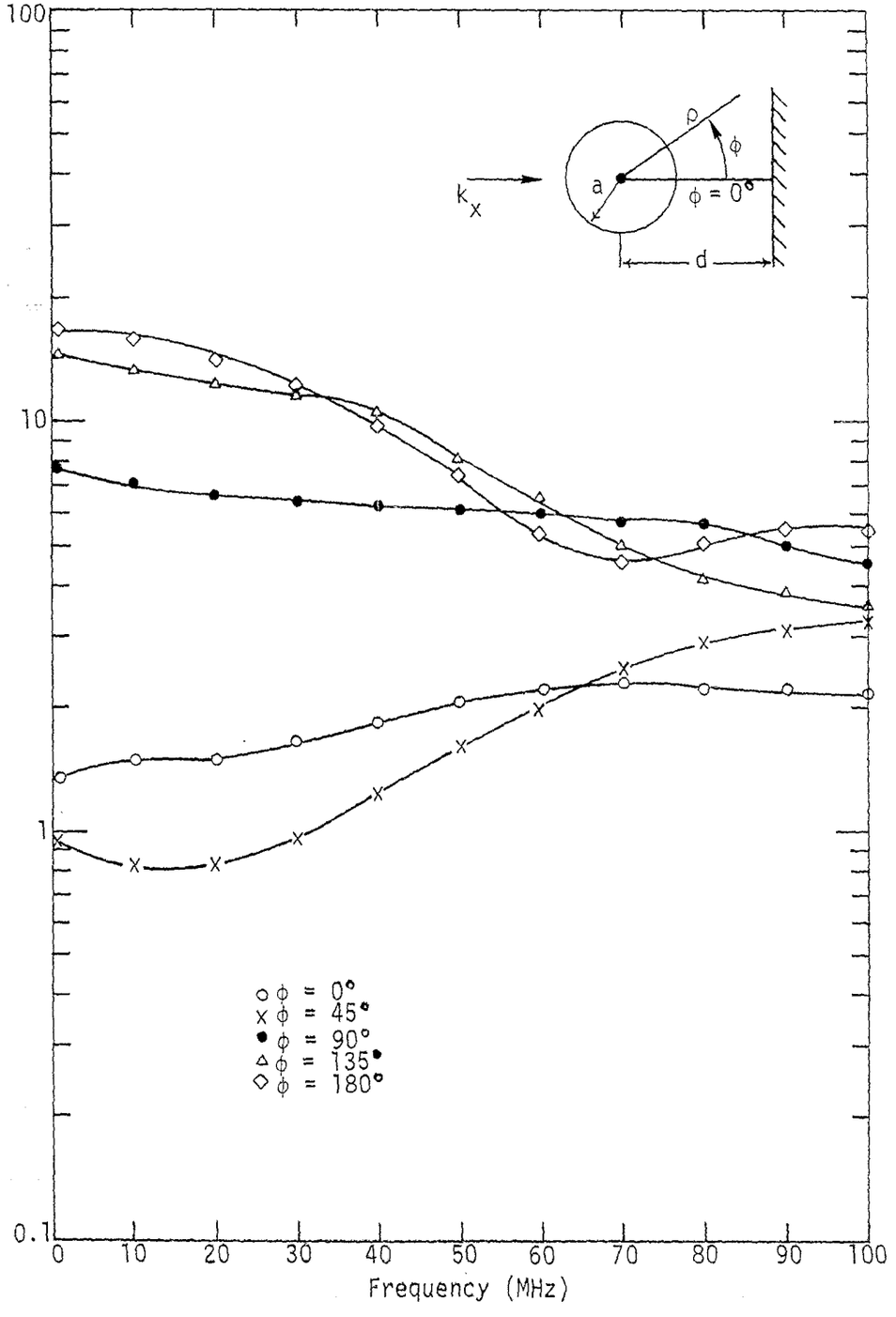

Figure 4c. $\left|J_z^{(HPD)}\right|$ as a function of frequency at different angle ϕ for a cylinder with a = 0.5 m, d = 1 m, calculated using second approximation.

The reason for this is that at low frequency, the first term in equation (19) dominates (which is a constant term) whereas the first term in equation (28) tends to be zero due to the reflected wave so that the second term dominates (which is proportional to cos ϕ).

In Figure 5, the function $Q1_i(\omega)$ is shown graphically for a cylinder with radius a = 0.5 m and d = 1 m. The variation is almost a factor of three in Figure 5a and a factor of five in Figure 5b.

In Figure 6, the function $Q1_i(\omega)$ is shown for the same cylinder at a distance d = 5 m away from the ground plane. For certain frequencies (e.g., 30 MHz, 60 MHz, 90 MHz), the incident and the reflected plane wave cancels so that a null in the graph is observed. This makes the error bounds difficult to estimate.

In Figure 7, an assumed relfected coefficient, REFL = -0.75, for an imperfect ground plane is used. For the case of a = 0.5 m, d = 1 m. The overall shape still has a factor of three variation.

In Figure 8, a different normalization is used before forming the ratio $R_i(\omega)$. The quantities $J_z^{(FF)}(\phi_i,\omega)$ are divided by $E_o e^{-jk\rho\cos\phi}$ at location (a, ϕ), and the quantities $J_A^{(HPD)}(\phi_i,\omega)$ are divided by the combination of incident and reflected wave, $E_o(e^{-jk\rho\cos\phi} - e^{-j2kd}\, e^{+jk\rho\cos\phi})$, at location (a, ϕ_i) and then the ratio $R_i(\omega)$ is formed. The resulting $Q1_i(\omega)$ seems to be worse than previous results if one looks at the variations.

A last example is to consider the ratio

$$R_i(\omega) = \frac{J_z^{(FF)}(\phi_i,\omega)}{J_z^{(FF)}(0°,\omega)} \tag{33}$$

and calculate the function $F1(\omega)$ and $Q1_i(\omega)$ according to equation (31) and (32). This is shown in Figure 9. This result indicates that the method applied to a cylinder in free space with two different angles of incidence will result in an error nearly a factor of three.

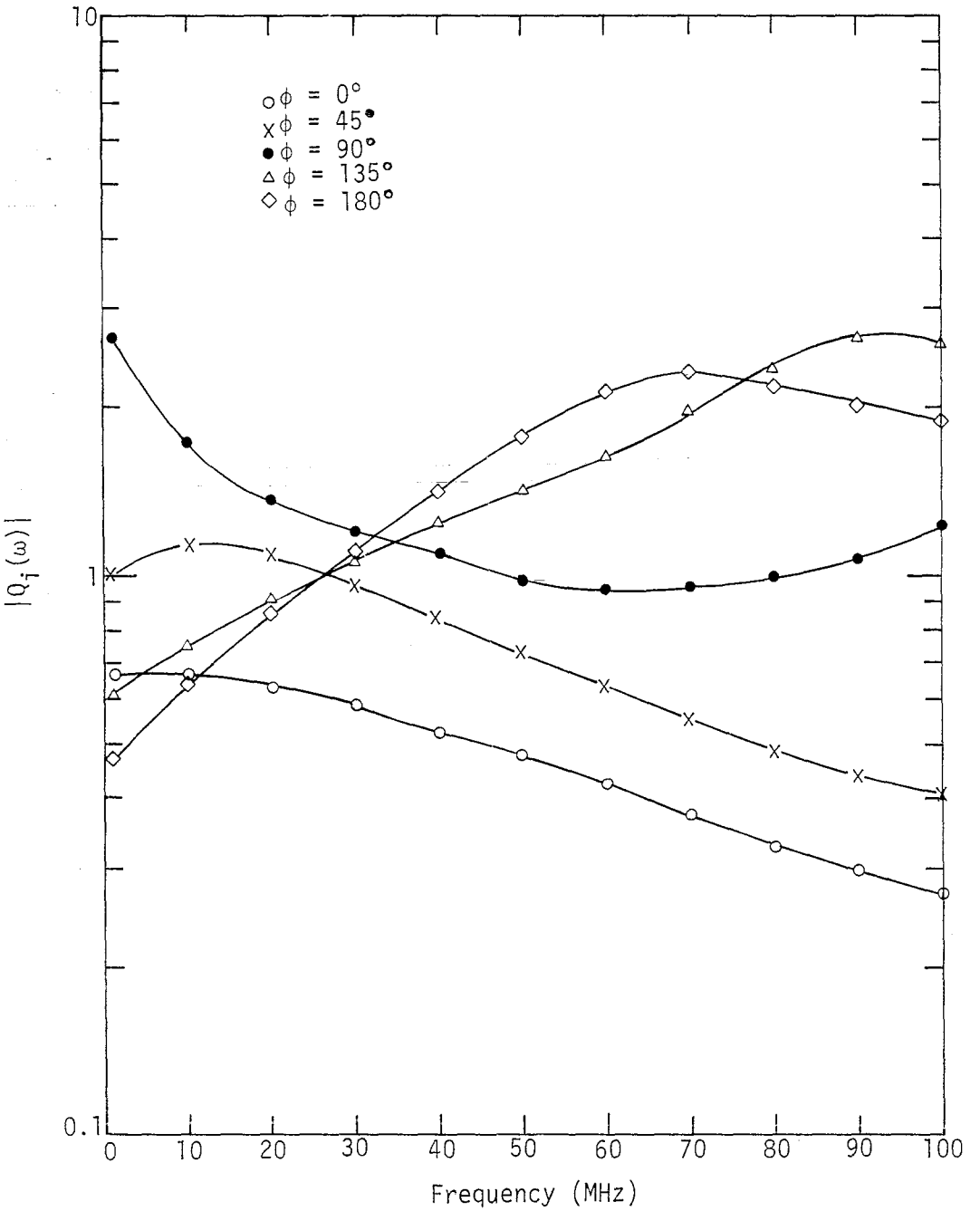

Figure 5a. The ratio $|Q_i(\omega)|$ at different angle ϕ_i calculated using first approximation and a reflection coefficient Refl = -1.0 for the ground, and a = 0.5 m, d = 1 m.

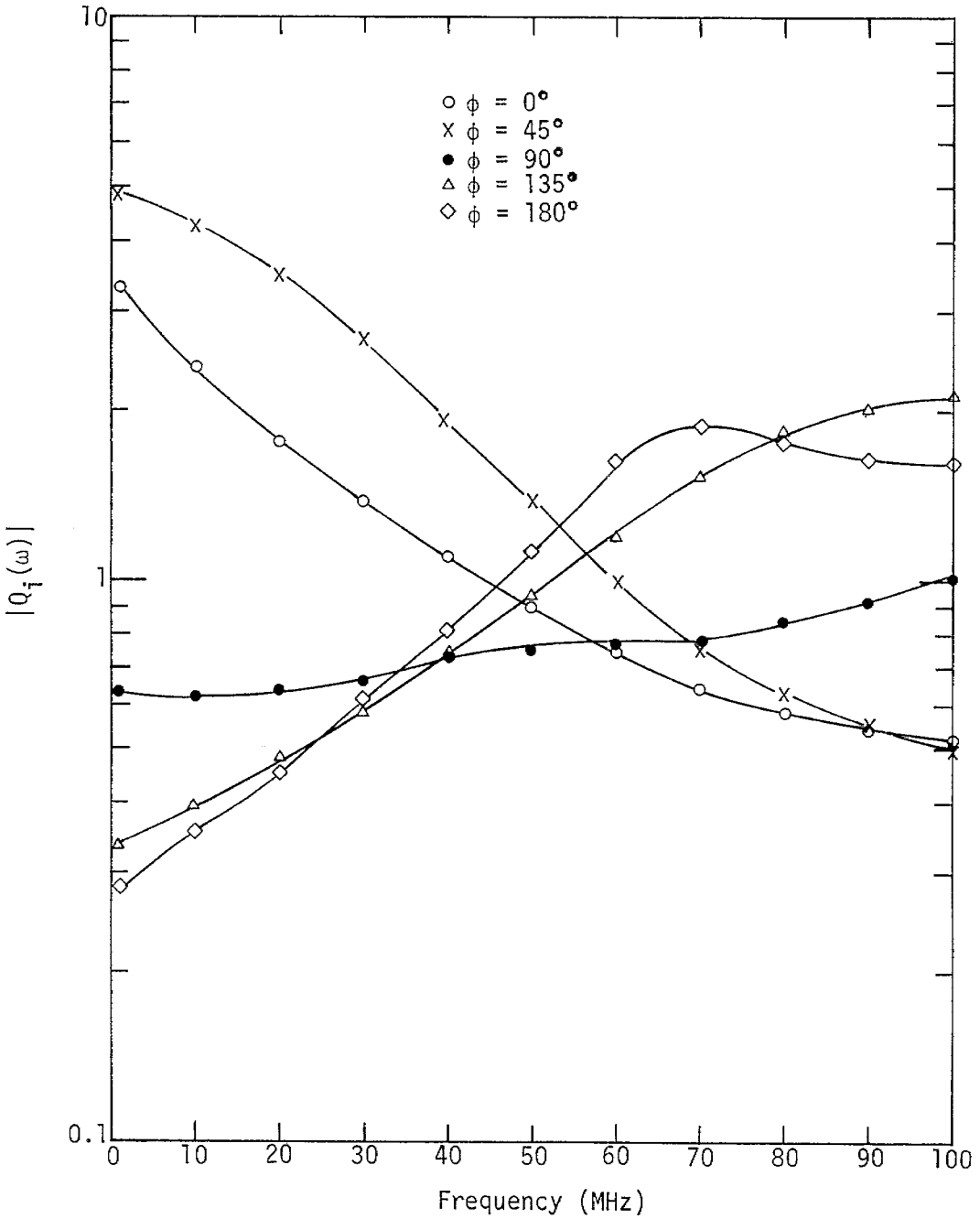

Figure 5b. The ratio $|Q_i(\omega)|$ calculated using second approximation and a reflection coefficient Refl = -1.0 for the ground, a = 0.5 m, d = 1 m.

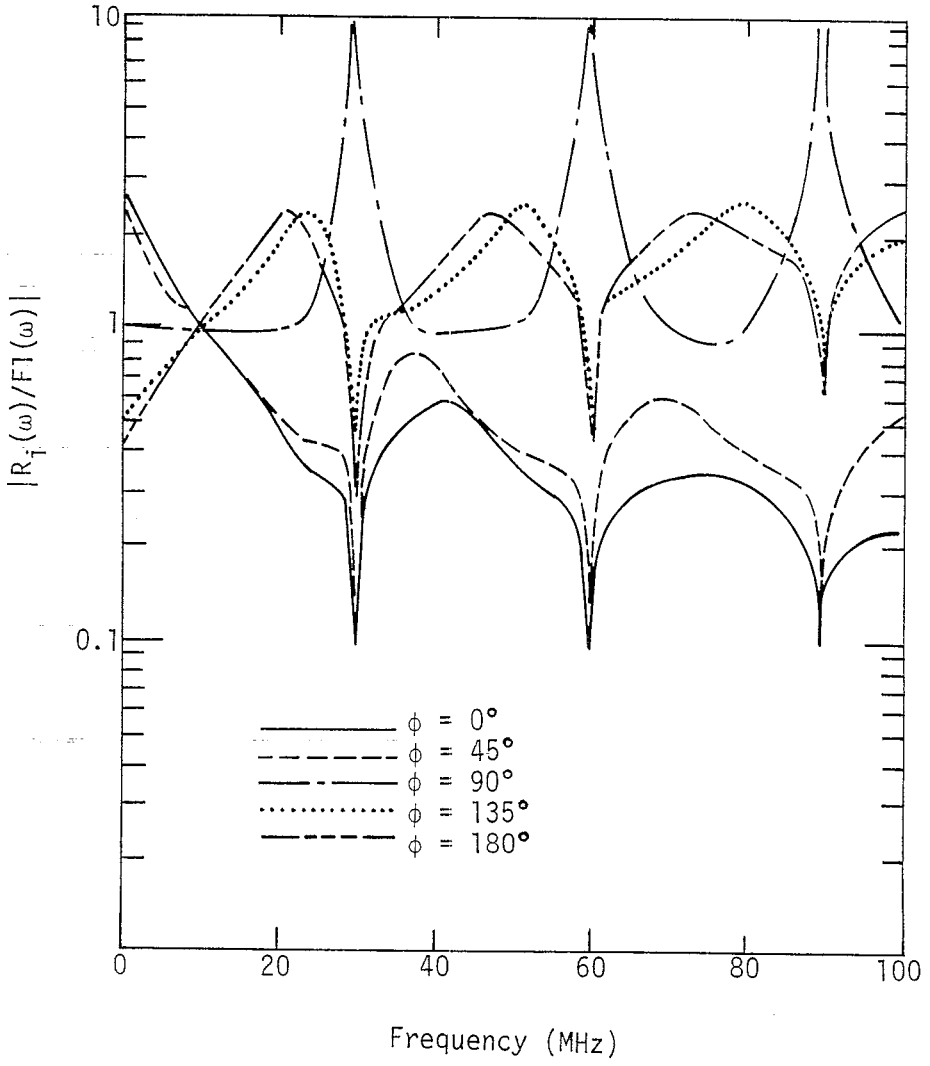

Figure 6. The ratio $|Q_i(\omega)|$ calculated using the first approximation and a reflection coefficient Refl = -1.0, a = 0.5 m, d = 5 m.

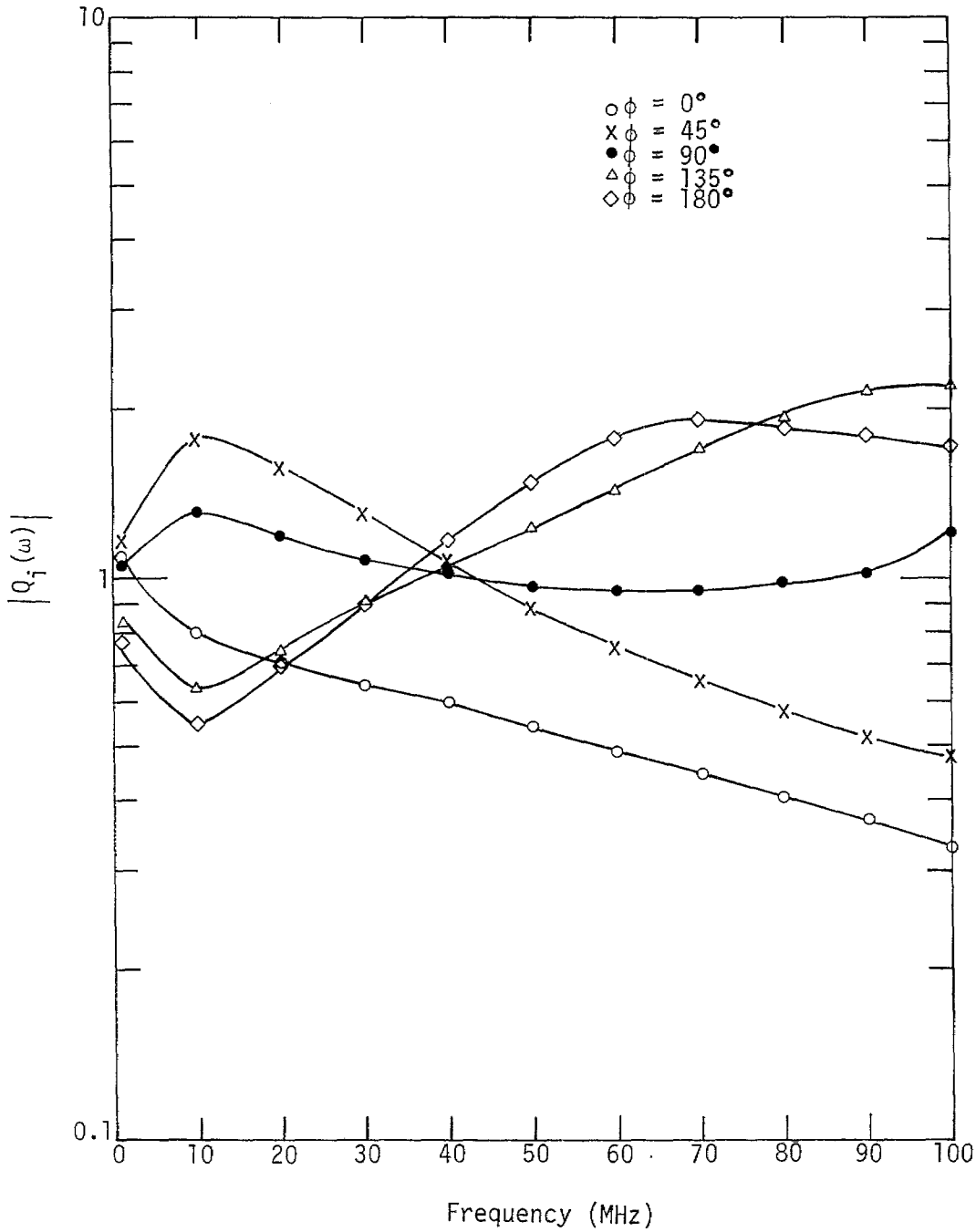

Figure 7a. The ratio $|Q_i(\omega)|$ at different angle ϕ_i calculated using first approximation and a reflection coefficient Refl = -0.75 for the ground, a = 0.5 m, d = 1 m.

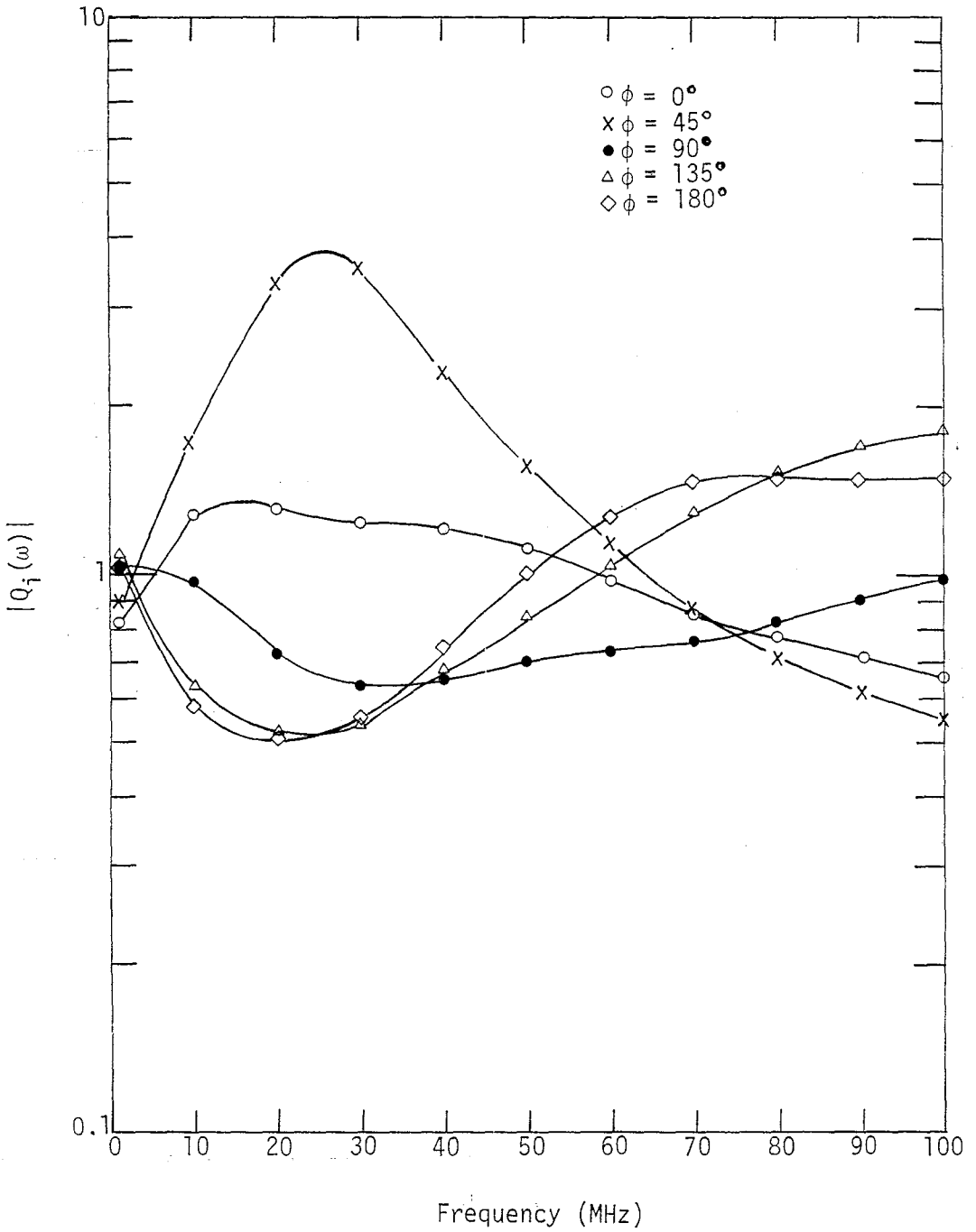

Figure 7b. The ratio $|Q_i(\omega)|$ at different angle ϕ_i calculated using second approximation and a reflection coefficient Refl = -0.75 for the ground, and a = 0.5 m, d = 1 m.

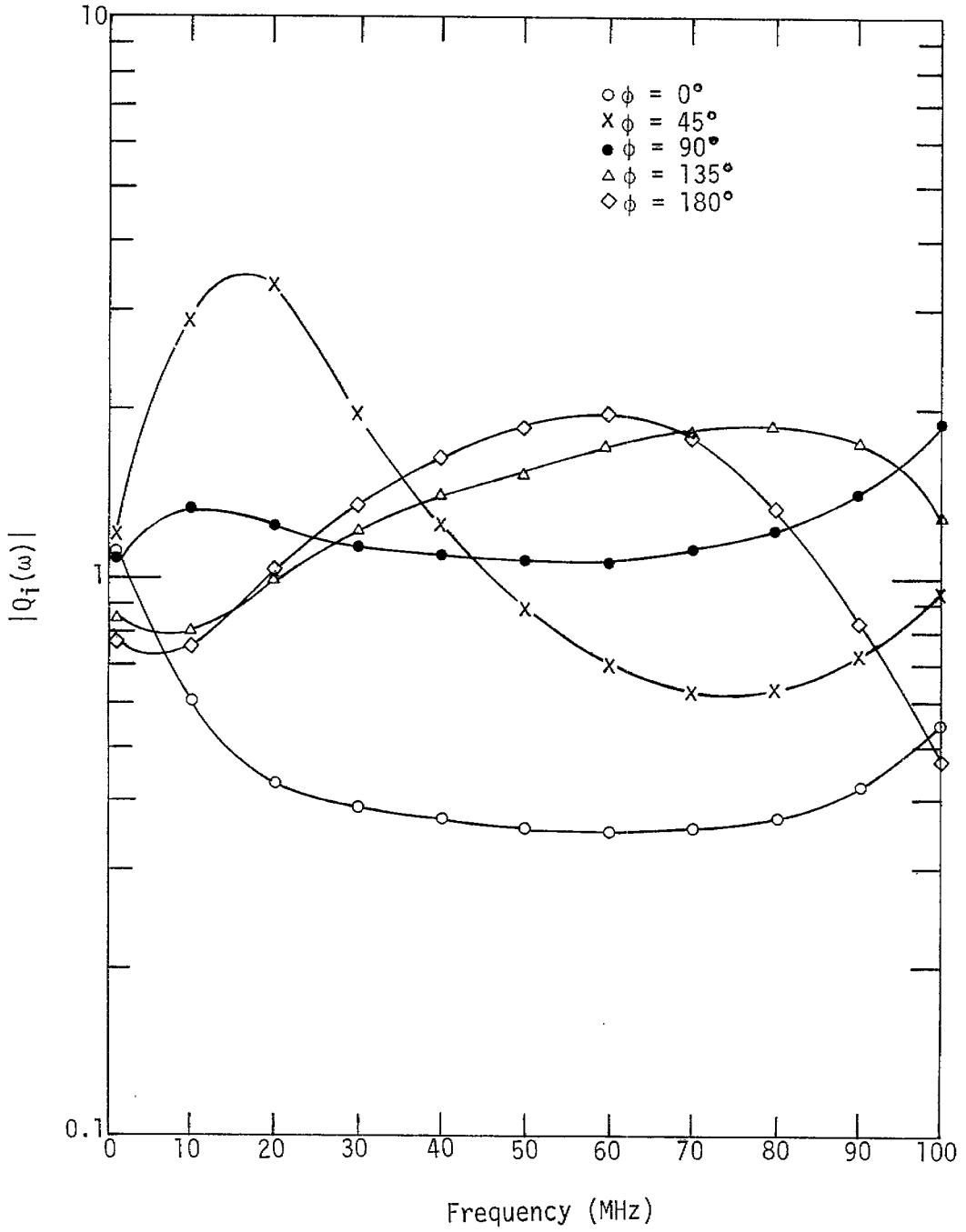

Figure 8. The ratio $|Q_i(\omega)|$ calculated using first approximation and a reflection coefficient Refl = -0.75 normalized to the incident field at different locations, a = 0.5 m, d = 1 m.

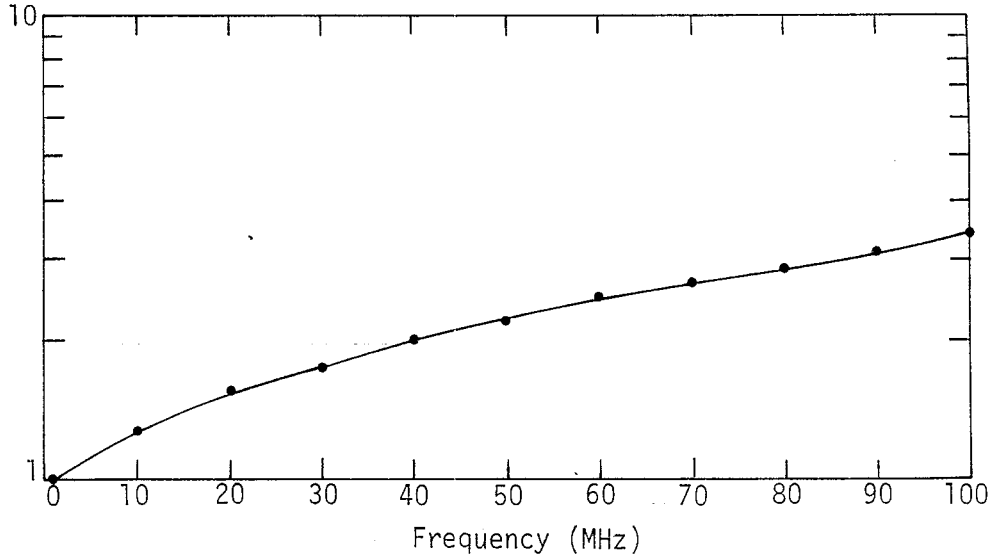

Figure 9a. The function $F1(\omega)$ for a cylinder in free space with a = 0.5 m.

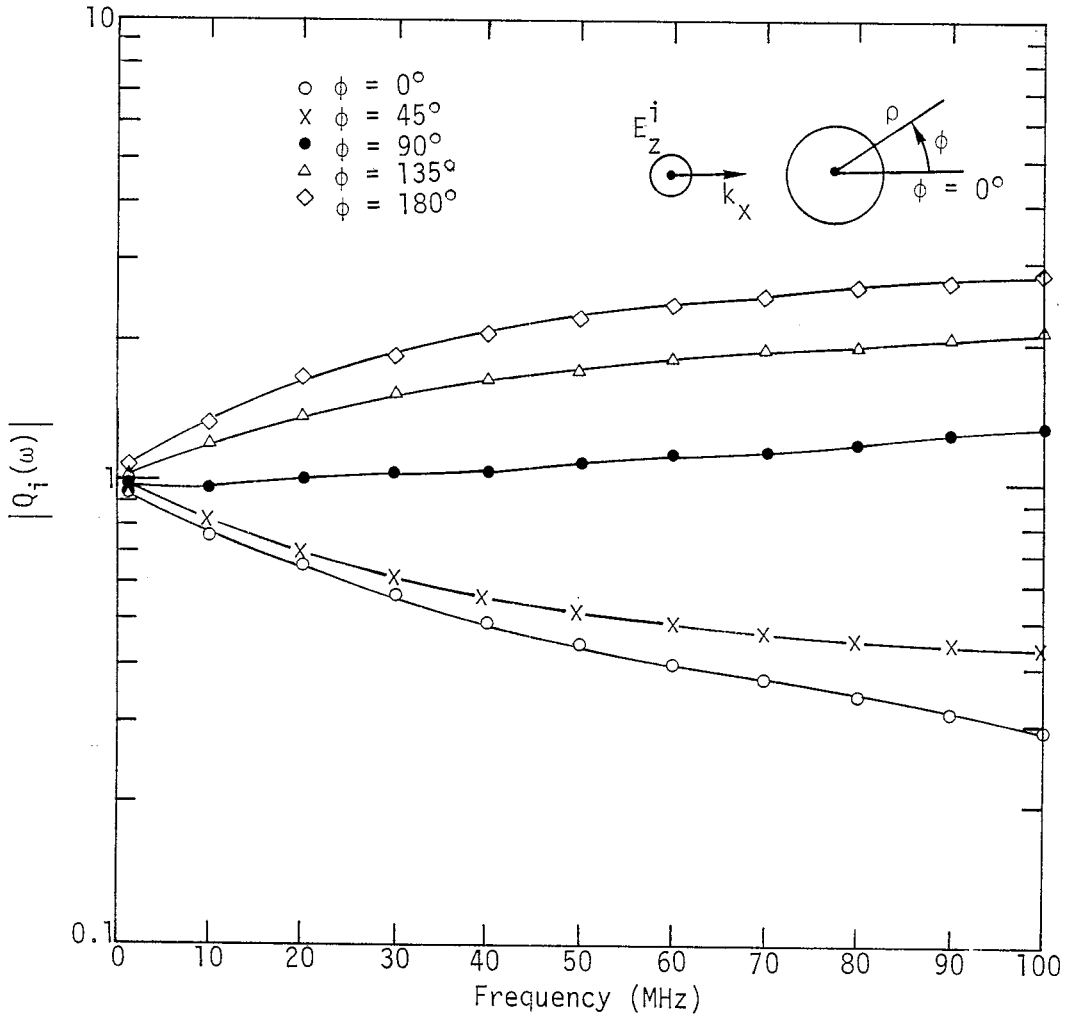

Figure 9b. The ratio $|Q_i(\omega)|$ for a cylinder with a = 0.5 m at different angle ϕ.

1.5 CONCLUSION

According to the discussion in the last section, the method of using an average extrapolation function $F1(\omega)$ to replace the individual extrapolation function $R_i(\omega)$ will result in an error of at least three to five times the correct results for that particular example. If the angle of incidence is not known and the comparison is made by selecting one arbitrary angle as reference, then the result could be subjected to an error as large as three times more. Since the example considered here is a simple two dimensional case, the result may or may not hold for the real airplane or three dimensional objects. However, it is highly unlikely that the error will be less if the object becomes more complex. For example, for a finite cylinder at resonance frequency, the currents near the center is very much larger than those near the ends. This brings in another error which could be larger than the variation as a function of angle. To estimate these errors, one would have to solve the exterior problem for each case and investigate the error bounds as illustrated in Section 1.4. It seems that the procedure is not general enough to be able to extrapolate information from one case to another unless one solves a similar problem. In other words, the specific results depend on the particular example and the boundary conditions used. This fact is not surprising since the principle of electrodynamic similitude is not fully obeyed in this method.

SECTION 2

'AN APPLICATION OF THE EXTRAPOLATION FUNCTION TECHNIQUE TO THE FINITE CYLINDER PROBLEM

2.1 INTRODUCTION

In Section 1 the motivations and the definitions of the method using extrapolation function in finding criteria response from simulation response are given. The method is then applied to a typical two-dimensional case of an infinite conducting cylinder in the presence of a plane incident wave with and without a ground plane. The result in that study indicates an error of a factor of nearly 3 to 5. In order to obtain a better estimation of the error bound concerning three dimensional objects and aircraft using this method, we extend the study to a cylinder with finite length in the presence of a plane incident wave in this report. The analytical solution of a finite cylinder in the presence of an incident wave is not easily available except when the cylinder is electrically thin (ref. 9). Numerical results have been obtained in several reports (refs. 10, 11, 12 and 13). The problem of a finite length cylinder with a ground plane in the presence of an incident field has not been studied extensively. The available results are those due to finite difference technique (ref. 14). In the next section, a brief summary of the numerical solutions of both problems using three dimensional finite difference method is given. These results are then used with the extrapolation function technique in the study of the error estimation.

2.2 FORMULATION OF THE FINITE CYLINDER PROBLEM (ref. 14, 12)

Figure 10 shows the configuration of a finite cylindrical conductor in the presence of an incident plane wave without a ground plane. The conductor is selected to be rectangular for convenience. The origin is

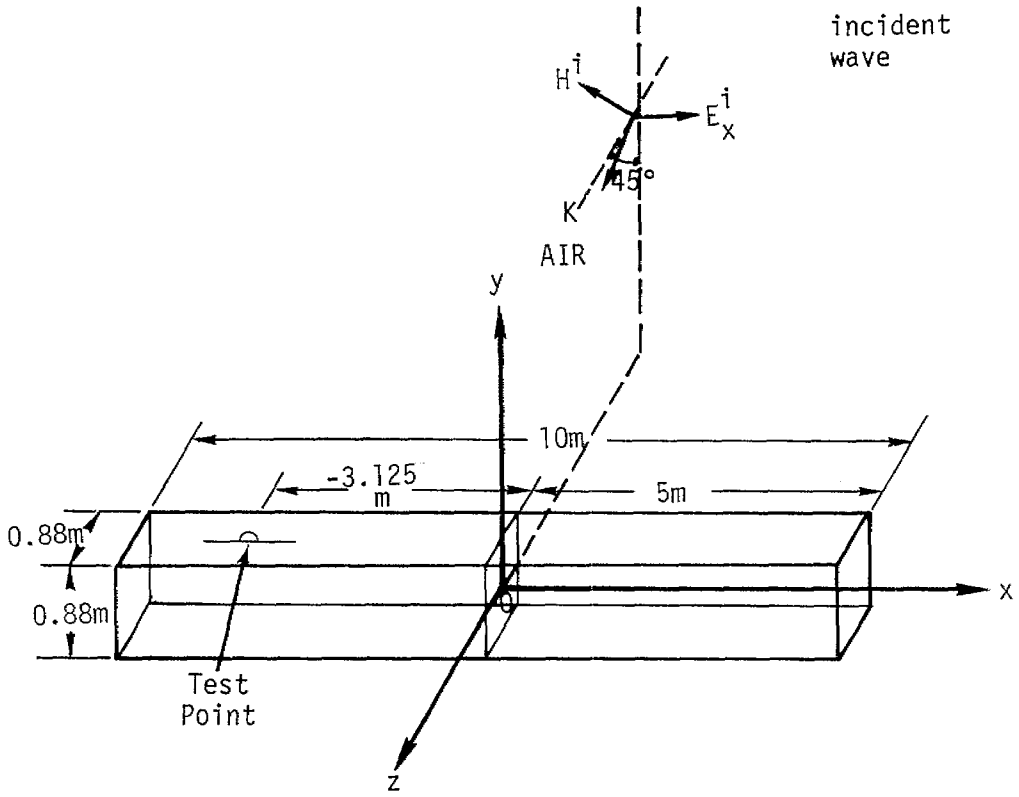

(a) Side View of the Pipe

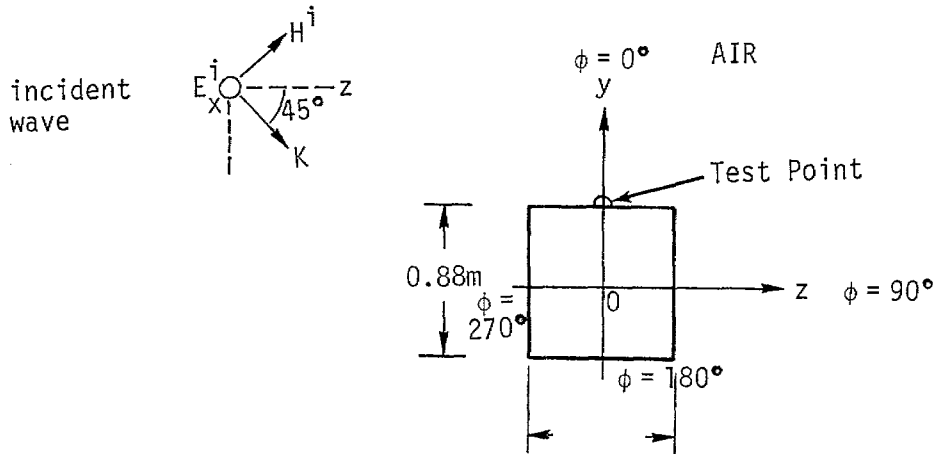

(b) Tail View of the Pipe

Figure 10. A finite cylindrical conductor in the presence of an incident plane wave without a ground plane.

the pipe center. An incident wave with an electric field E^i parallel to the x-axis and a $\hat{k}$-vector forming a 45° angle with both y-axis and z-axis was selected for some practical reason. In the calculation, the length of the pipe is 10 m and the width is 0.88 m as shown in Figure 10. The corresponding configuration of a finite cylinder in the presence of an incident plane wave with a ground plane is shown in Figure 11. The parameters of the ground are assumed to be $\varepsilon_r = 10$ and $\sigma = 0.02$. The pipe is located at a height d = 1 m above the ground in the sample calculation. The incident plane wave is taken to be $E^{inc}(t) = 5.94\times10^4\times[e^{-4.08\times10^6 t} - e^{-3.50\times10^8 t}]$.

To use the finite difference method to solve for the electromagnetic fields, the Maxwell equations are expressed in a three-dimensional finite difference form. The scattered field caused by the pipe is found by solving these finite-difference equations subject to the boundary conditions. The boundary conditions are (1) on the surface of the pipe, $E^{scatt}_{tan}(t) = -E^{inc}_{tan}(t)$, (2) inside the pipe, $E^{scatt}(t) = 0$, (3) appropriate radiation conditions are applied on the outer boundary of the space.

The induced surface current on the pipe is given by $\vec{J} = \vec{n}\times\vec{H}$, where $\vec{H} = \vec{H}^{scatt} + \vec{H}^{inc}$ is the total magnetic field at the desired location. A detailed discussion of the implementation of this method is given in other reports (refs. 14 and 2) and will not be repeated here. It is noted that, using this method, the response of the finite cylinder with a ground plane can also be determined approximately if an assumed reflection coefficient is used for the ground. Since the response is calculated in time domain using this method, a Fourier transformation has to be used in order to obtain the response as a function of frequency. In the following calculation, the reflection coefficient for the ground is assumed to be $Refl = -1 + 0.25\ e^{-t/200\times10^{-9}}$ with t in sec.

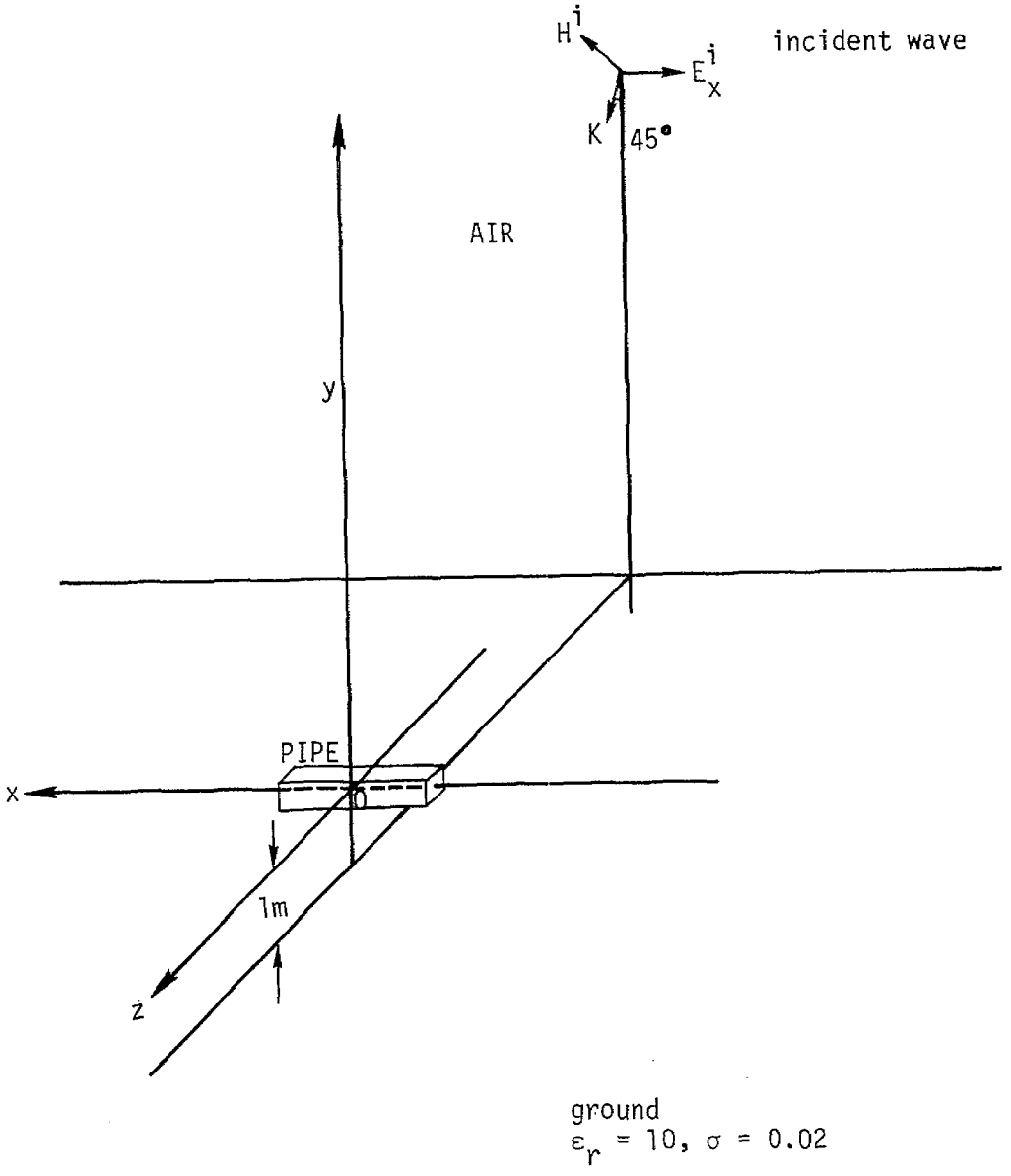

Figure 11. A finite cylindrical conductor in the presence of an incident plane wave with a ground plane. The dimensions of the pipe are given in Figure 10.

2.3 APPLICATION OF THE EXTRAPOLATION FUNCTION TO THE FINITE CYLINDER PROBLEM

Making use of the definitions and notations given in Section 1, the following extrapolation function is obtained,

$$R_i(\omega) = \frac{\tilde{J}_x^{(FF)}(\phi_i,\omega)}{\tilde{J}_x^{(ATH)}(\phi_i,\omega)} \tag{34}$$

where $\tilde{J}_x^{(FF)}(\phi_i,\omega)$ is the axial current density obtained for the case without a ground plane (Figure 10) in frequency domain, and $\tilde{J}_x^{(ATH)}(\phi_i,\omega)$ is the axial current density obtained for the case with a ground plane (Figure 11) in frequency domain. An average function $F1(\omega)$ is formulated as follows,

$$F1(\omega) = \sqrt[N]{R_1(\omega)\ R_2(\omega)\ R_3(\omega)\ \ldots\ R_N(\omega)} \quad . \tag{35}$$

Then, the following ratio is calculated and plotted as a function of frequency,

$$Q1_i(\omega) = \frac{R_i(\omega)}{F1(\omega)} \quad . \tag{36}$$

In all the examples given below, N = 4 and i = 1,2,3,4 corresponding to a test point located at ϕ_i = 0°, 90°, 180° and 270° (see Figure 10b) at the position x respectively.

In Figure 12, the axial current density $J_x^{(FF)}(0°,t)$ is shown as a function of time. The corresponding Fourier transformation is shown in Figure 13. A "tail" has been added to the time-domain response from 550 nsec to 1000 nsec in order to minimize the resulting error in the Fourier transform. Also, in Figure 12, the axial current density $J_x^{(FF)}(90°,t)$ is shown. The corresponding Fourier transform is shown in Figure 13.

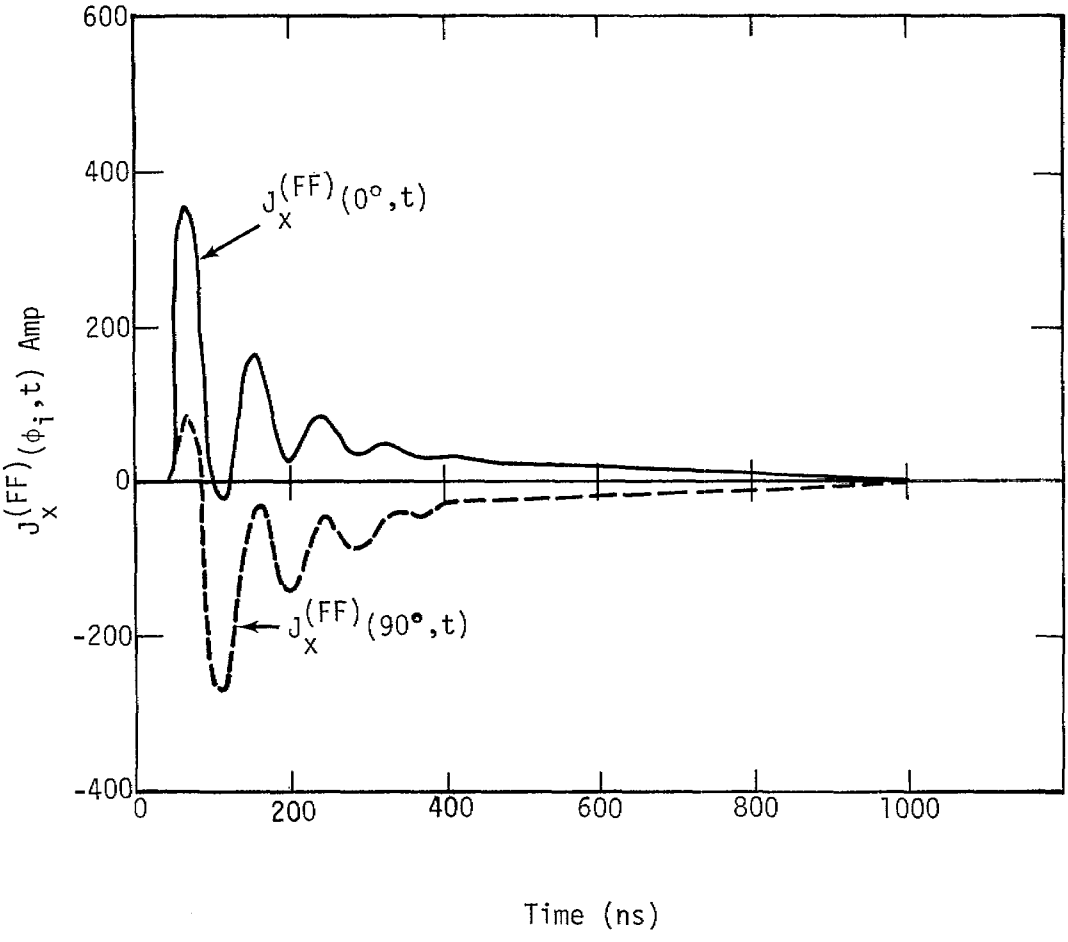

Figure 12. The axial current density $J_x^{(FF)}(\phi_i,t)$ at x = -3.125 m.

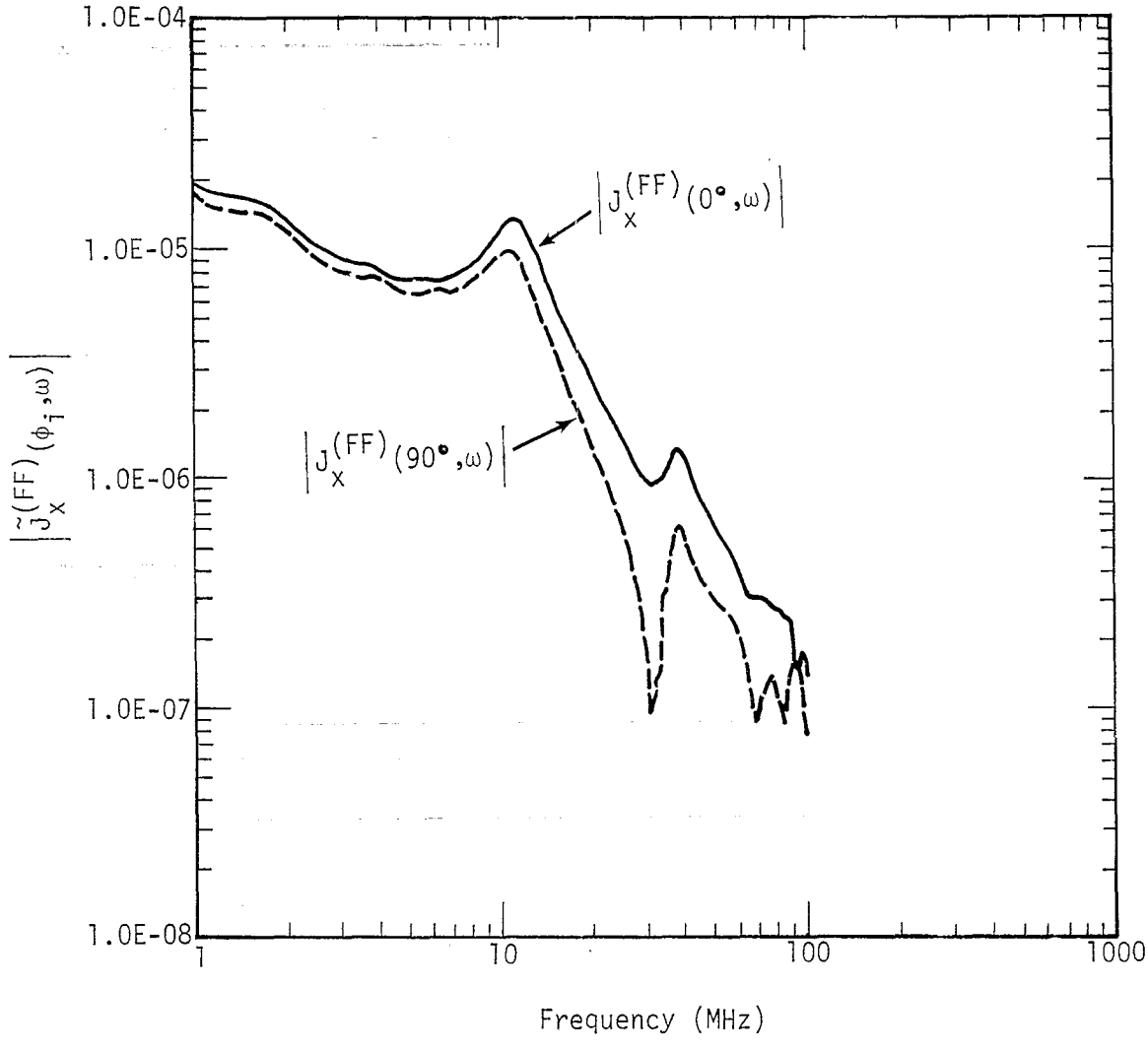

Figure 13. The magnitude of the Fourier transform of $J_x^{(FF)}(\phi_i,t)$ at x = -3.125 m.

Note that in the case of a cylinder in free space, $J_x^{(FF)}(0°,t) = J_x^{(FF)}(270°.t)$, and $J_x^{(FF)}(90°,t) = J_x^{(FF)}(180°,t)$ due to the incident field selected and the symmetry configuration as shown in Figure 10. (All the above curves are calculated at x = -3.125 m).

Next, let us consider the ratio,

$$R_i(\omega) = \frac{\tilde{J}_x^{(FF)}(\phi_i,\omega)}{\tilde{J}_x^{(FF)}(\phi_i + 90°,\omega)} \tag{37}$$

and calculate the function $F1(\omega)$ and $Q1_i(\omega)$ according to equation (35) and equation (36). This equivalent to applying the extrapolation function technique to a cylinder in free space for two plane incident wave with incident angles differing by 90°. The function $|Q1_i(\omega)|$ is shown in Figure 14. Note that $Q1_i(\omega) = Q1_i(\omega) = 1$ due to symmetry. The function $Q1_i(\omega)$ is the inverse of $Q1_i(\omega)$, which can be easily deduced from their definitions. The combination of all these curves shows a variation of a factor near 10. On the same graph, typical values obtained by using Sancer's code (ref. 11) are also shown in open and closed dots. They agree with the results of 3-D code. In using Sancer's code, the incident wave is taken to be an impulse, and the cylinder in free space is a circular cylinder with radius a = 0.5 m and length 10 m. This cylinder has the same volume as that used in 3-D code. These two results are comparable since the normalized quantities (i.e., the ratio of two responses) are used in the calculation.

In Figure 15, the axial current density $J_x^{(ATH)}(\phi_i,t)$ is shown for ϕ_i = 0°, 90°, 180°, 270° at x = -3.125 m. The corresponding Fourier transforms are shown in Figure 16. The current $J_x^{(ATH)}(0°,t)$ is not equal to $J_x^{(ATH)}(270°,t)$, and $J_x^{(ATH)}(90°,t)$ is not equal to $J_x^{(ATH)}(180°,t)$ because the presence of the ground plane disturbs the symmetry conditions.

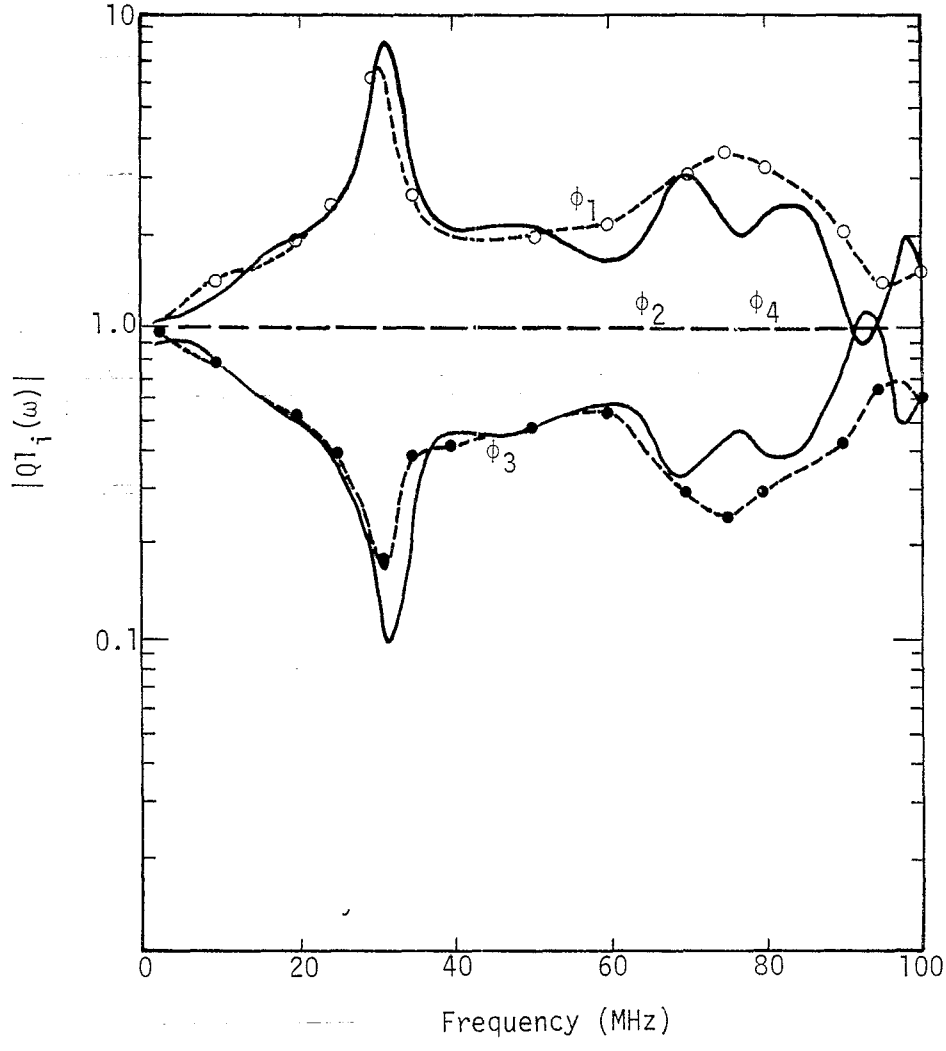

Figure 14a. The ratio $|Ql_i(\omega)|$ for a cylinder in free space for two incident waves with incident angle different by 90°.

——— calculated using 3-D code

--o-- calculated using Sancer's code

--•--

with $\phi_1 = 0°$, $\phi_2 = 90°$, $\phi_3 = 180°$, $\phi_4 = 270°$.

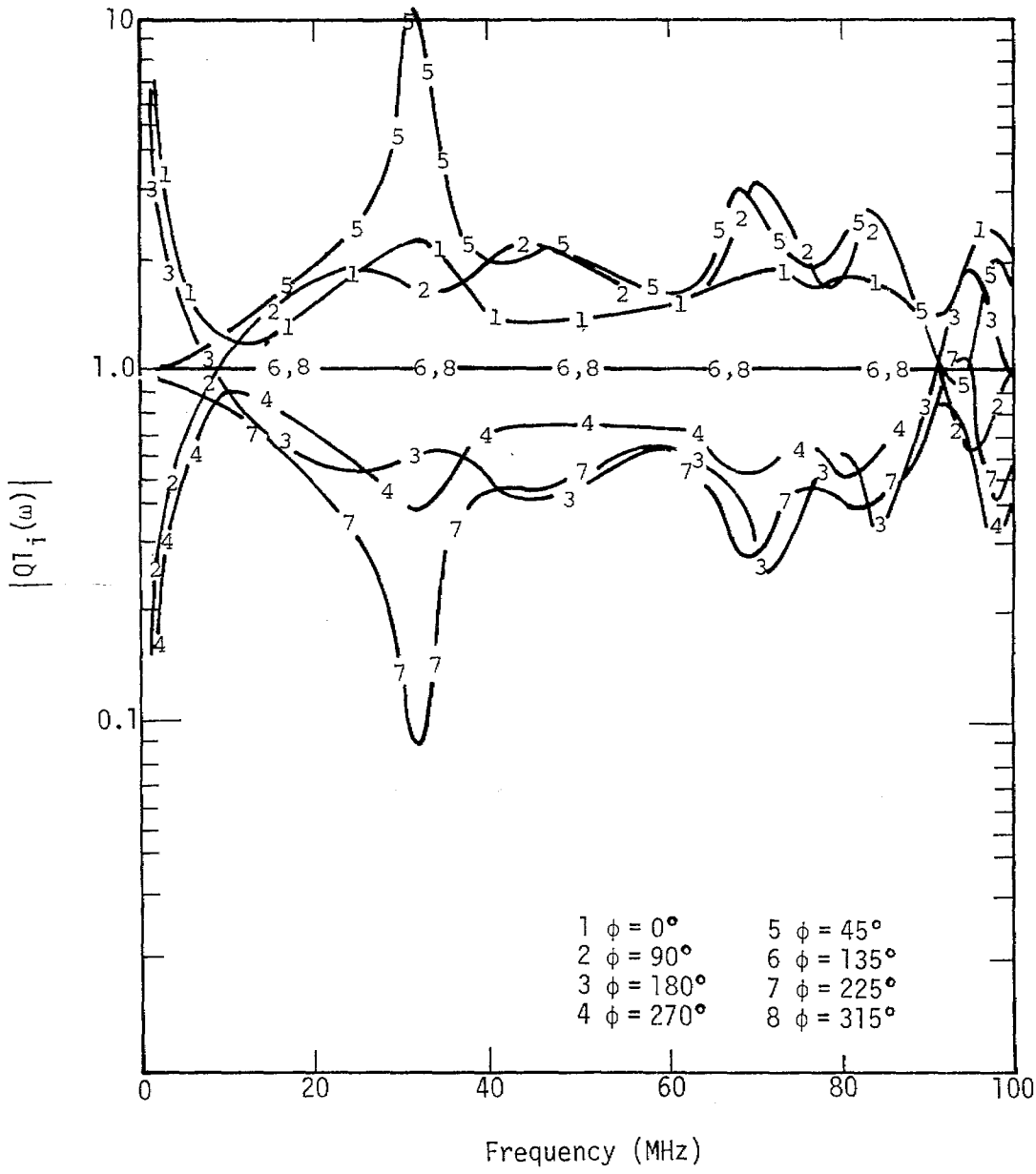

Figure 14b. The ratio $|Ql_i(\omega)|$ for a cylinder in free space for two incident waves with incident angle different by 90°, calculated using 3-D code.

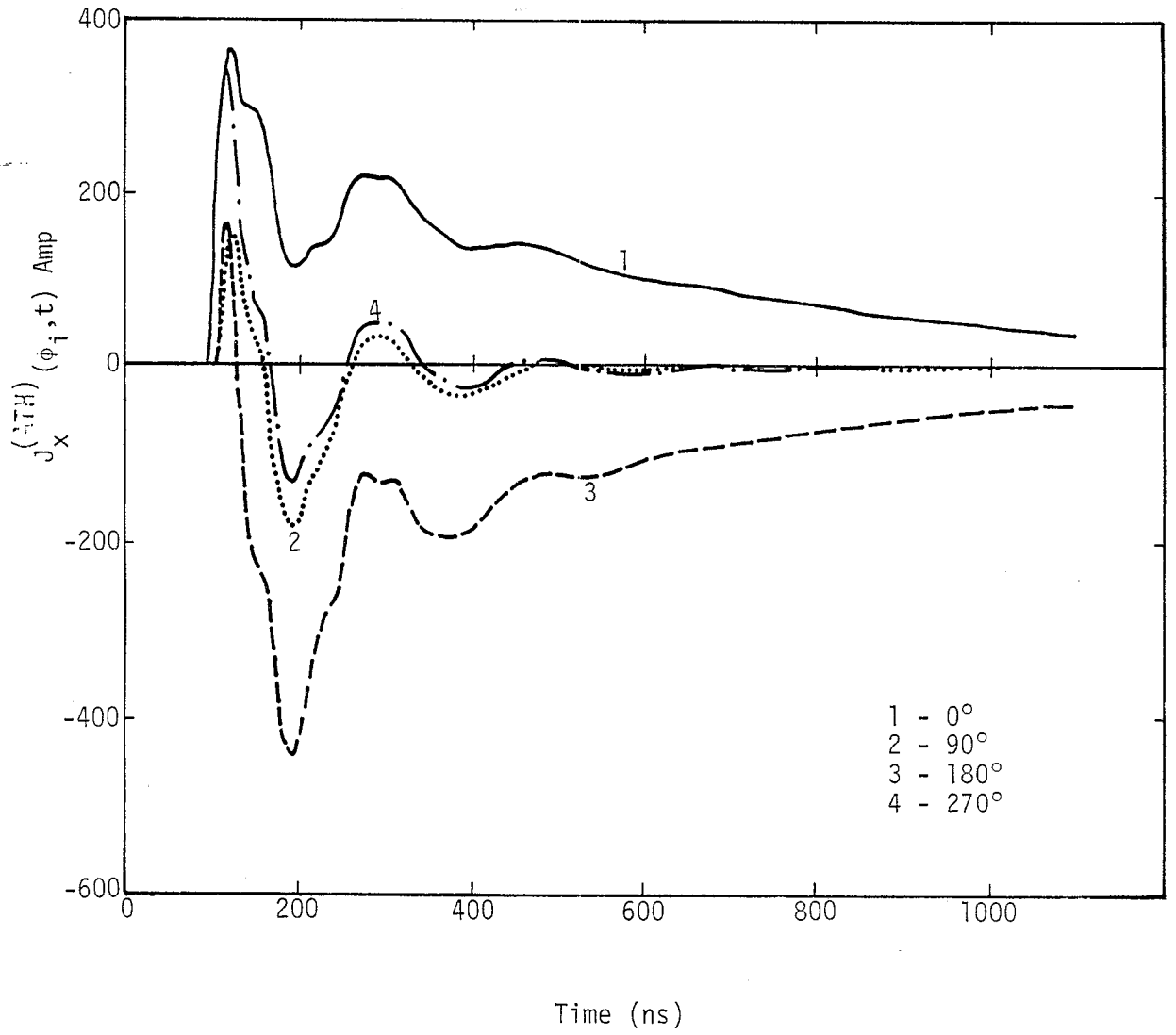

Figure 15. The axial current density $J_x^{(ATH)}(\phi_i,t)$ at x = -3.125 m.

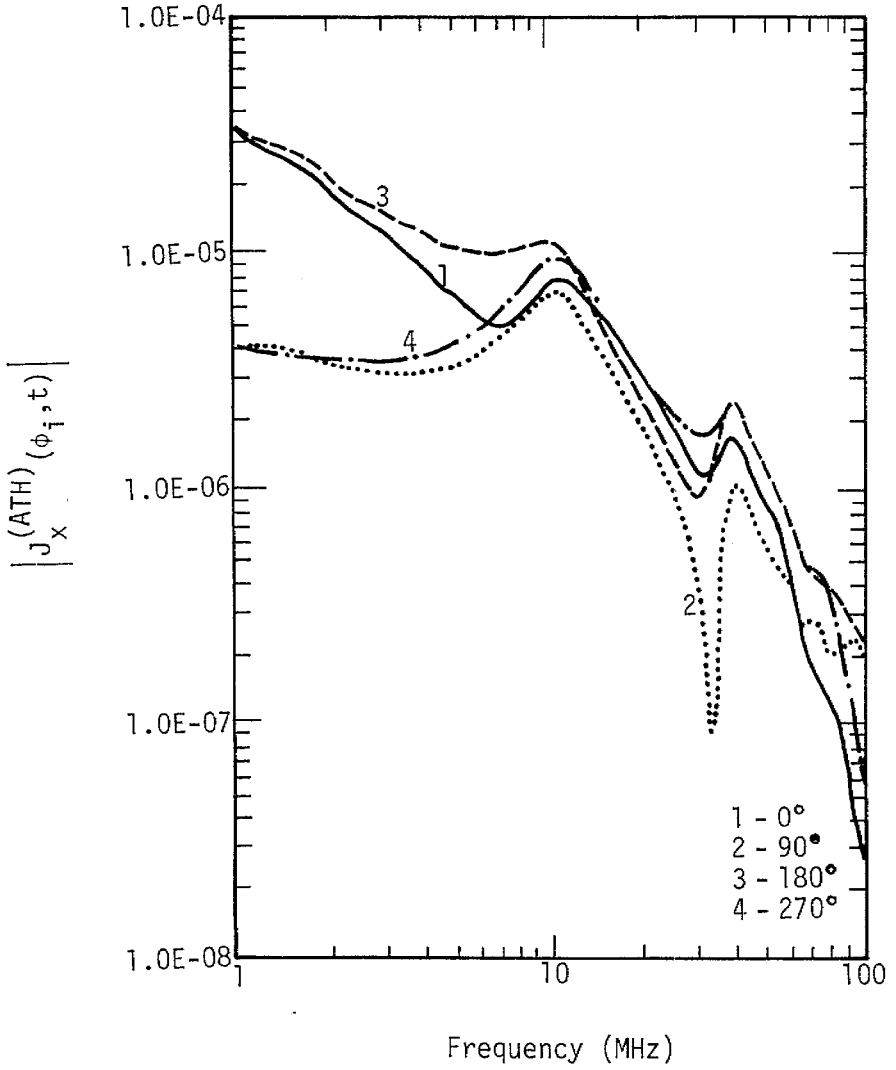

Figure 16. The magnitude of the Fourier transform of $J_x^{(ATH)}(\phi_i,t)$ at x = -3.125 m.

In Figure 8, the ratio

$$R_i(\omega) = \frac{\tilde{J}_x^{(FF)}(\phi_i,\omega)}{\tilde{J}_x^{(ATH)}(\phi_i,\omega)} \tag{38}$$

is used to calculate the function $|Q1_i(\omega)|$ according to equation (35) and equation (36). It is seen that the function $|Q1_i(\omega)|$ is not a constant at low frequency end, which is similar to the results obtained for the infinite cylinder problem in reference 8. The total variation over the frequency range from 1 MHz to 100 MHz is nearly a factor of 5 as shown in Figure 17.

In Figure 18, the Fourier transforms $|\tilde{J}_x^{(FF)}(\phi_i,\omega)|$ at x = 0 are shown, and in Figure 19, the Fourier transforms $|\tilde{J}_x^{(ATH)}(\phi_i,\omega)|$ at x = 0 are shown. The calculated $|Q1_i(\omega)|$ using these curves and equations (34), (35) and (36) is shown in Figure 20. The variation over the frequency range from 1 MHz to 100 MHz is roughly a factor of 6.

2.4 CONCLUSION

In conclusion, when the extrapolation concept is generalized and applied to a cylinder in free space for two incident waves with 90° difference, it shows an error of about a factor of 10. When the method is applied to compare the currents on the cylinder in free space and those on the cylinder near a ground plane, it shows an error of nearly a factor of 6. As pointed out in the concluding remarks in reference 8, this kind of error is due to the difference in the boundary condition and cannot be removed effectively unless the boundary conditions are modified to be similar to each other in the two problems.

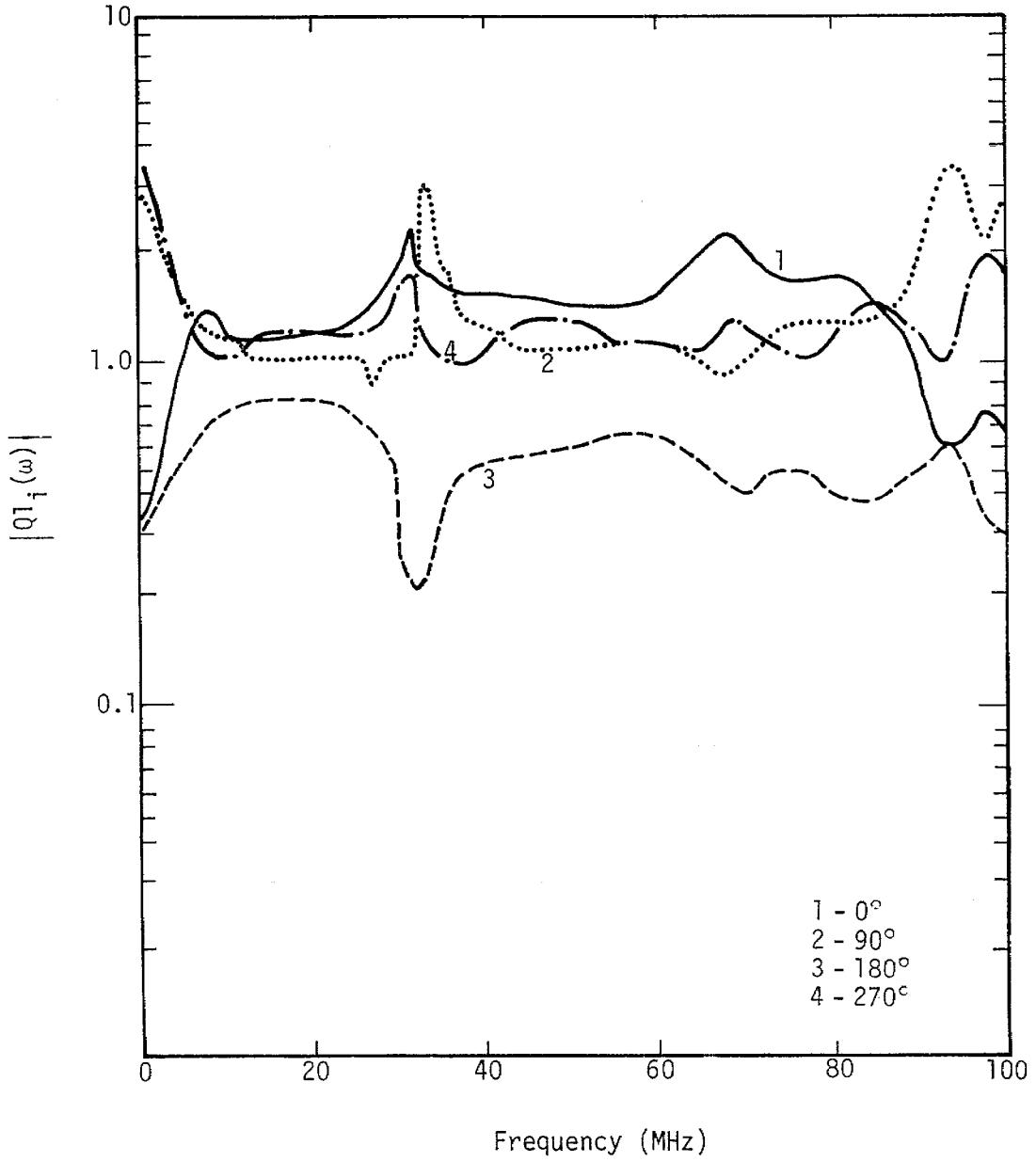

Figure 17. The ratio $|Q1_i(\omega)|$ at different angle ϕ_i at x = -3.125 m, using data given in Figure 13 and Figure 16.

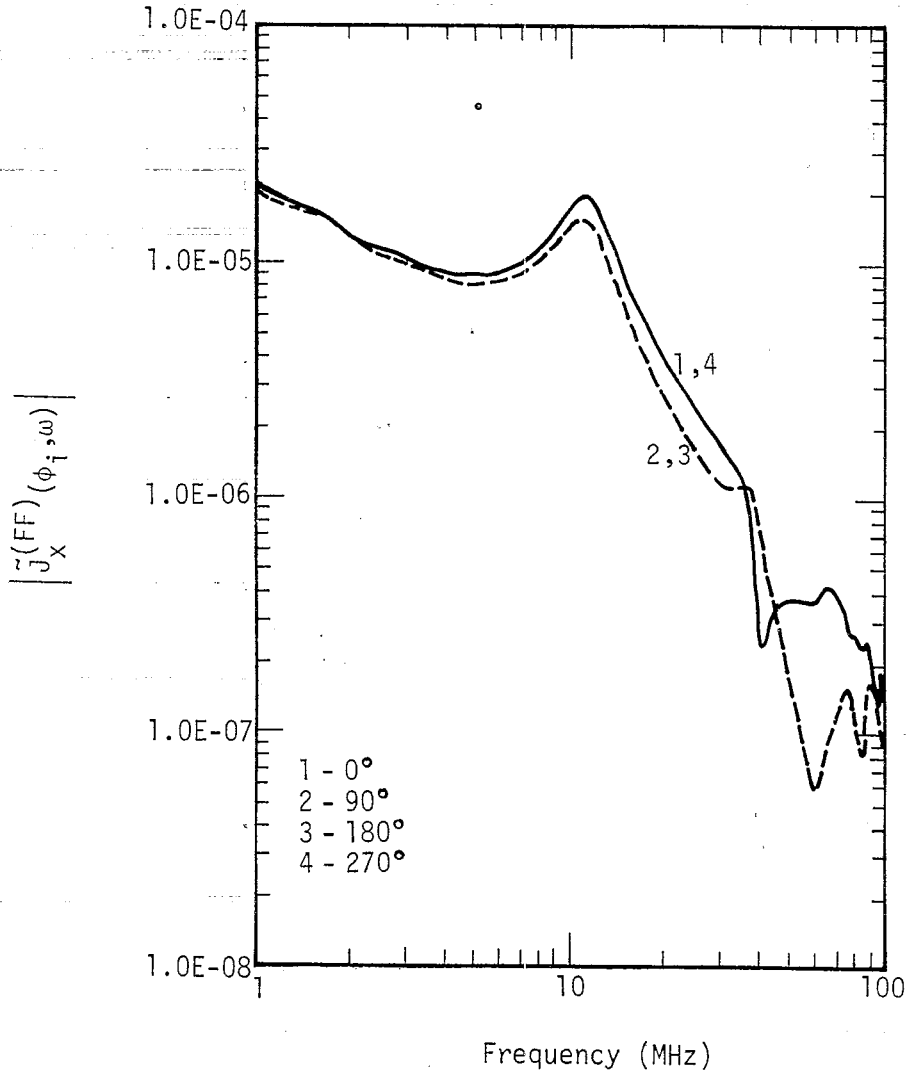

Figure 18. The magnitude of the Fourier transform $\tilde{J}_x^{(FF)}(\phi_i,\omega)$ at x = 0 m.

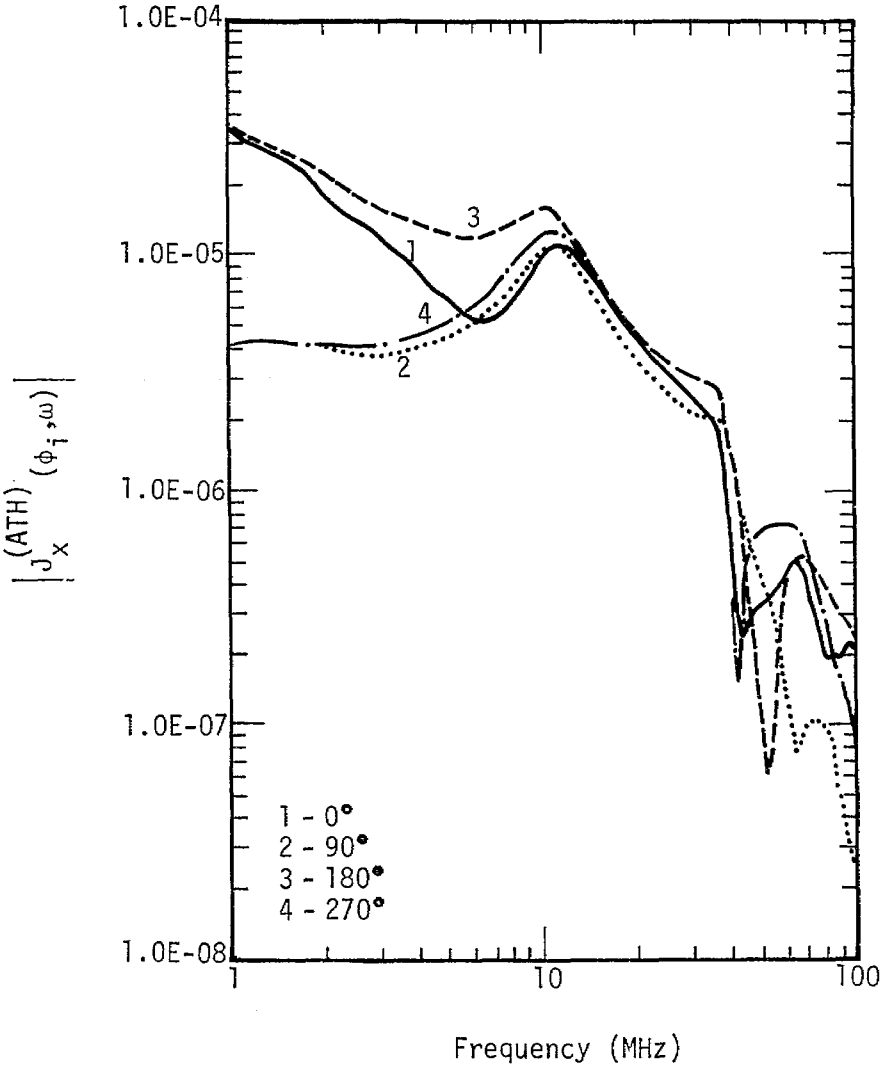

Figure 19. The magnitude of the Fourier transform $\tilde{J}^{(ATH)}(\phi_i,\omega)$ at x = 0 m.

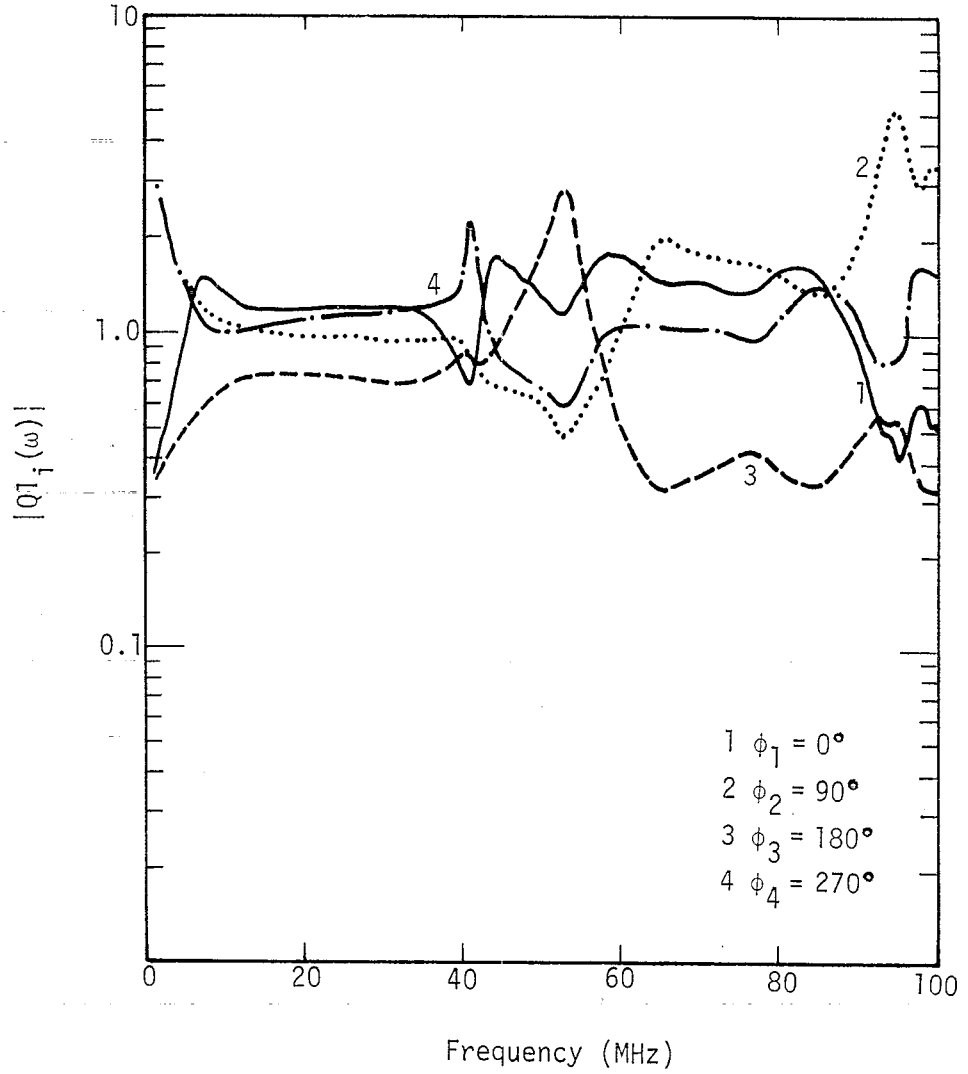

Figure 20. The ratio $|Q1_i(\omega)|$ at different angle ϕ_i at x = 0 m, using data given in Figure 18 and Figure 19.

SECTION III

THE INFINITE CYLINDER PROBLEM IN THE PRESENCE OF A PLANE WAVE WITH DIFFERENT INCIDENT ANGLE

3.1 SCATTERING OF AN INFINITE CONDUCTING CYLINDER FOR AN INCIDENT WAVE WITH INCIDENT ANGLE β

Considering Figure 21, an infinite cylindrical conductor is illuminated by a plane incident wave with incident angle β as shown. Let the incident wave have its electric field component E_z parallel to the axis of the cylinder (z-axis). Mathematically, the incident field can be written as

$$E_z^i = E_o \, e^{-jk\rho \cos(\beta-\phi)} \, e^{+j\omega t} \quad . \quad (39)$$

The scattered field E_z^s due to the cylinder can be determined by expanding the scattered and incident fields in terms of cylindrical wave functions and using the boundary condition $E_z^{total} = E_z^i + E_z^s = 0$ at $\rho = a$. The result is (with $e^{+j\omega t}$ suppressed)

$$E_z^s = -E_o \sum_{n=\infty}^{\infty} \frac{J_n(ka)}{H_n^{(2)}(ka)} \, j^{-n} \, H_n^{(2)}(k\rho) \, e^{-jn(\beta-\phi)} \quad . \quad (40)$$

The total magnetic field is then,

$$H_\phi^{total} = \frac{1}{j\omega\mu} \frac{\partial E_z^{total}}{\partial \rho} \quad . \quad (41)$$

The current density on the cylinder is given by

$$J_z = H_\phi^{total} \text{ , at } \rho = a \quad . \quad (42)$$

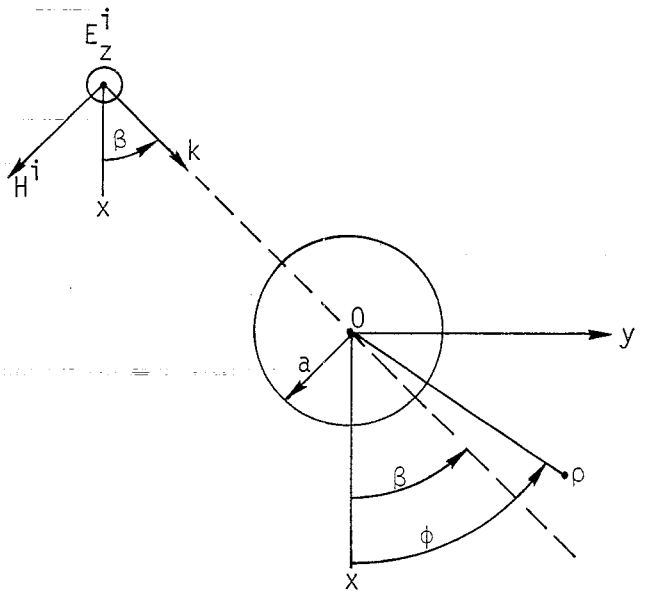

Figure 21. An infinite cylindrical conductor in the presence of an incident plane wave with incident angle β.

Combining (39), (40), (41), and (42), it can be shown that

$$J_z = \frac{2E_o}{\omega\mu\pi a} \sum_{n=\infty}^{\infty} j^{-n} \frac{e^{-jn(\beta-\phi)}}{H_n^{(2)}(ka)} \tag{43}$$

3.2 AN INFINITE CONDUCTING CYLINDER WITH A PERFECT CONDUCTING GROUND PLANE IN THE PRESENCE OF AN INCIDENT PLANE WAVE WITH INCIDENT ANGLE β

Considering Figure 22, an infinite cylindrical conductor with a perfect conducting plane is illuminated by a plane incident wave with incident angle β.

Let R_1 be the reflection coefficient ($R_1 = -1$ for perfect conductor), and let

$$E_z^i = E_o \sum_{n=-\infty}^{\infty} j^{-n} J_n(k\rho)\, e^{-jn(\beta-\phi)} \tag{44}$$

$$E_z^r = R_1 E_o\, e^{-j2kd\cos\beta} \sum_{n=-\infty}^{\infty} j^{+n} J_n(k\rho)\, e^{+jn(\beta+\phi)} \tag{45}$$

$$E_z^s = E_o \sum_{n=-\infty}^{\infty} a_n j^{-n} H_n^{(2)}(k\rho)\, e^{+jn\phi} \tag{46}$$

$$E_z^{sr} = R_1 E_o \sum_{n=-\infty}^{\infty} a_n j^{+n} \sum_{m=-\infty}^{\infty} H_m^{(2)}(2kd)\, J_{n+m}(k\rho)\, e^{-jn\phi-jm\phi} \tag{47}$$

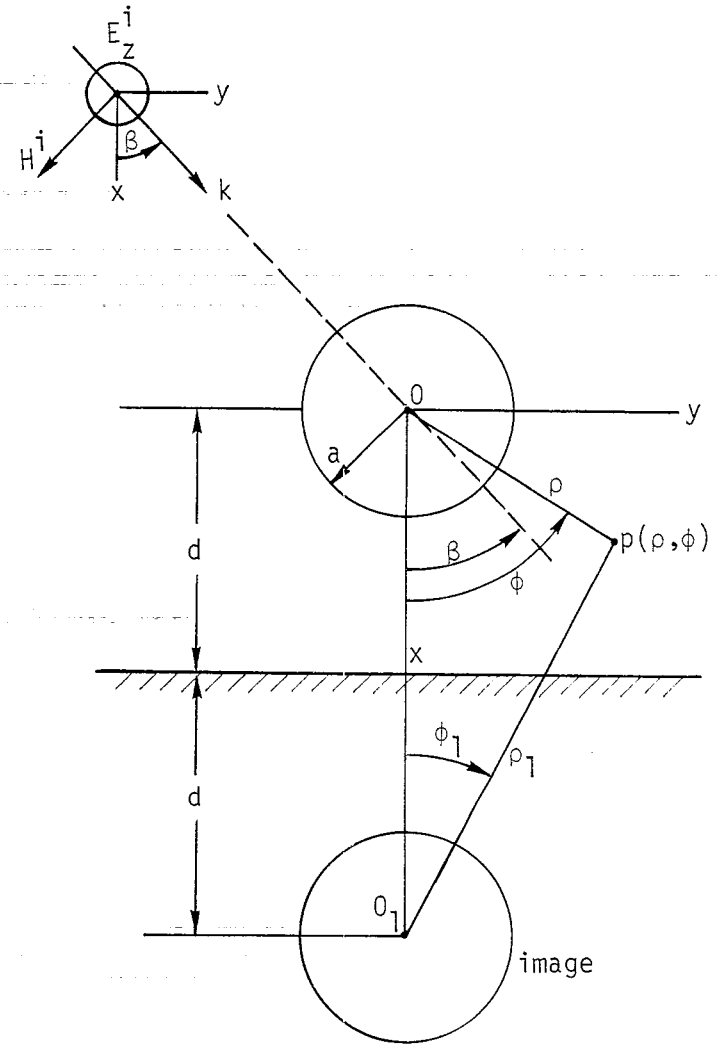

Figure 22. An infinite cylindrical conductor with a ground plane in the presence of an incident plane wave with incident angle β.

$$E_z^{total} = E_z^i + E_z^r + E_z^s + E_z^{sr} \tag{48}$$

where E_z^{total} is the total electric field in the space, E_z^i is the plane incident wave expanded in cylindrical wave functions, E_z^r is the reflected plane wave due to the ground expanded in cylindrical wave functions, E_z^s and E_z^{sr} are scattered fields due to the cylinder and its image with the unknown constant a_n. It can be easily shown that, on the ground plane ($x = d$), $E_z^{total} = 0$ using (44), (45), (46), (47) and (48) and the additional theorem of Bessel's functions.

The constant a_n can be determined by the following boundary condition,

$$E_z^{total} = 0, \quad \text{at } \rho = a \tag{49}$$

From (44) through (48) it is found that

$$\sum_{n=-\infty}^{\infty} j^{-n} J_n(ka)\, e^{-jn(\beta-\phi)} + R_1\, e^{-j2kd\cos\beta} \sum_{n=-\infty}^{\infty} j^{+n} J_n(ka)\, e^{+jn(\beta+\phi)}$$

$$+ \sum_{n=-\infty}^{\infty} a_n\, j^{-n} H_n^{(2)}(ka)\, e^{+jn\phi}$$

$$+ R_1 \sum_{n=-\infty}^{\infty} j^{+n} a_n \sum_{m=-\infty}^{\infty} H_m^{(2)}(2kd)\, J_{n+m}(ka)\, e^{-jn\phi-jm\phi} = 0 \tag{50}$$

Rearranging the last summation and collecting terms associated with $e^{+jn\phi}$, we find the following equation for determining a_n,

$$j^{-n}\, a_n\, H_n^{(2)}(ka) + R_1\, j^{-n}\, a_{-n}\, H_o^{(2)}(2kd)\, J_{-n}(ka)$$

$$+\sum_{m=1}^{\infty} R_1\, j^{-(n+m)} a_{-(n+m)} H_m^{(2)}(2kd) J_{-n}(ka)$$

$$+\sum_{m=1}^{\infty} R_1\, j^{m-n} a_{m-n} H_m^{(2)}(2kd)(-1)^{m-n} J_n(ka)$$

$$= -(j^{-n}\, e^{-jn\beta} + R_1\, e^{-j2kd\, \cos\beta}\, j^{+n_e+jn\beta})\, J_n(ka) \quad . \qquad (51)$$

For simplicity, we consider an approximation with $H_m^{(2)}(2kd)\, J_n(ka)$ terms neglected in (51). This is equivalent to neglect the effects due to the image cylinder. When this is done, one finds

$$a_n \cong -\frac{\left(j^{-n_e-jn\beta} + R_1\, e^{-j2kd\, \cos\beta}\, j^{+n_e+jn\beta}\right) J_n(ka)}{j^{-n}\, H_n^{(2)}(ka)} \quad . \qquad (52)$$

Using (52), (44) through (48), (41) and (42), the current density is given by

$$J_z \cong \frac{2E_o}{\omega\mu\pi a} \sum_{n=-\infty}^{\infty} \frac{(j^{-n_e-jn(\beta-\phi)} + R_1\, e^{-j2kd\, \cos\beta}\, j^{+n_e+jn(\beta+\phi)})}{H_n^{(2)}(ka)} \quad . \qquad (53)$$

3.3 CONSIDER A SPECIAL CASE

Assuming that the infinite cylinder is an ideal version of certain "two-dimensional airplane" so that, in Figure 21, the airplane is in the

free space and in Figure 22 the airplane is near a ground plane. When the "airplane" is illuminated by an incident EMP wave, the electromagnetic energy can be coupled into the "airplane" body through the possible port of entry. This coupling energy is related to the current density J_z through some transfer functions. We shall consider a case where the incident wave can come from any angle β with $-\pi/2 \leq \beta \leq \pi/2$.

Let $J_z^{(FF)}(\phi_j,\beta_k)$ be the current density given in (43) and $J_z^{(HPD)}(\phi_j,\beta_k)$ be that given in (53), where ϕ_j is the location of the current density on the cylinder (with radius a), and β_k is the angle of incidence. Let a maximum number be defined from a set of k numbers as follows:

$$J_z(\phi_j)_{max} = \max\left\{J_z(\phi_j,\beta_1),\ J_z(\phi_j,\beta_2),\ \ldots,\ J_z(\phi_j,\beta_k)\right\} . \qquad (54)$$

At a particular angle ϕ_j, we only select one current density, $J_z(\phi_j)_{max}$, due to certain incident field among all the possible incident waves, and assuming this quantity will dominate the coupling effect. For $j = 1, \ldots, m$, we obtained a set of numbers which contains the maximum current density at each particular location when β_k is varied. Thus, from $J_z^{(HPD)}(\phi_j,\beta_k)$ we have the following set

$$A = \left\{J_z^{(HPD)}(\phi_1)_{max},\ J_z^{(HPD)}(\phi_2)_{max},\ \ldots,\ J_z^{(HPD)}(\phi_m)_{max}\right\}. \qquad (55)$$

Note that β_k can only be varied in $-\pi/2 \leq \beta_k \leq \pi/2$.

Similarly, we can construct a set of numbers $J_z^{(FF)}(\phi_j)_{max}$ from $J_z^{(FF)}(\phi_j,\beta_k)$. In order to make a fiar comparison, we restrict β_k in this case also between $-\pi/2$ to $+\pi/2$. From the result of part one in this section, it is not hard to see that the maximum current density for an infinite cylinder illuminated by a plane wave occurs at the illuminated side. For example, when the wave is coming from $\phi_j = 180°$ with $\beta_k = 0°$, the maximum current density is that located at $\phi_j = 180°$. Since we allow the incident

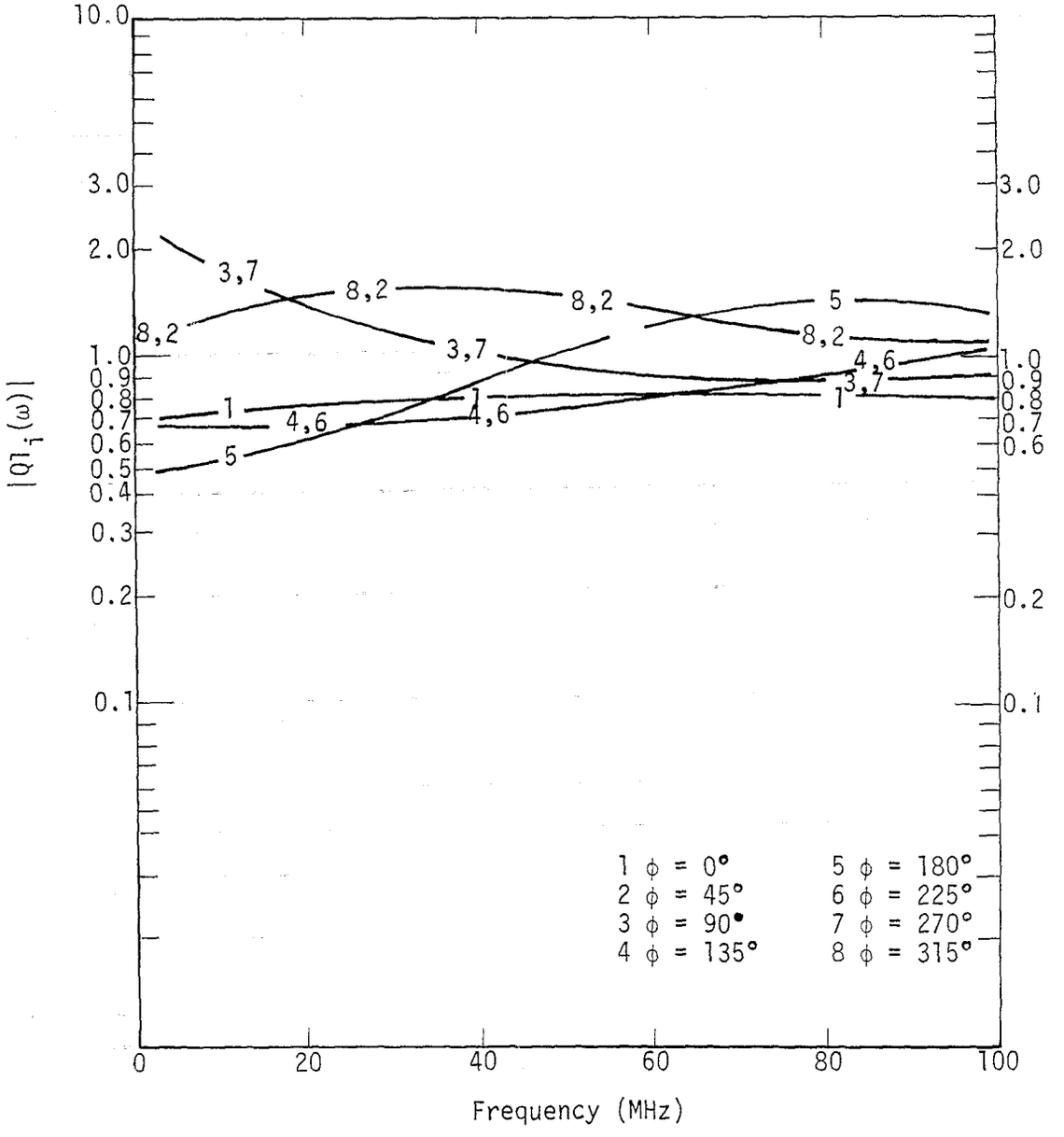

Figure 23. The ratio $|Q1_i(\omega)|$ at different angle ϕ_i with a = 0.5 m, d = 1 m, $R_1 = -1.0$ and $\beta = -\pi/4, 0, \pi/4$.

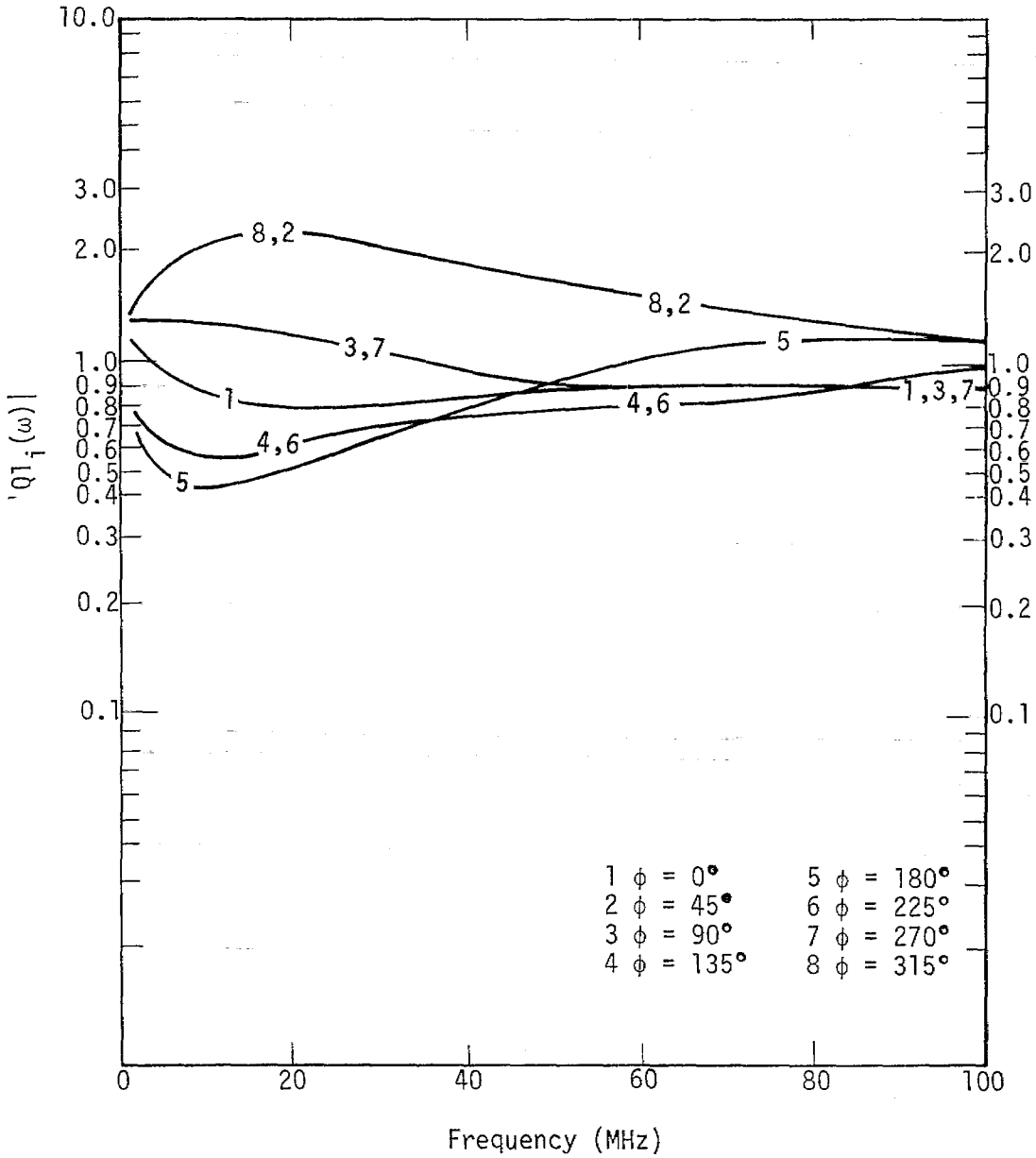

Figure 24. The ratio $|Q1_i(\omega)|$ at different angle ϕ_i with a = 0.5 m, d = 1 m, $R_1 = -0.75$ and $\beta = -\pi/4, 0, \pi/4$.

fields to be varied from $\beta_k = -\pi/2$ to $+\pi/2$, the maximum current density will be a constant equal to $J_z^{(FF)}(180°,0°)$ for $\pi/2 \leq \phi_j \leq 3\pi/2$. The current density in the shadow side can also be determined easily. Thus, the following set can be obtained from $J_z^{(FF)}(\phi_j,\beta_k)$ for $j = 1, 2, \ldots, m$

$$B = \left\{ J_z^{(FF)}(\phi_1)_{max},\ J_z^{(FF)}(\phi_2)_{max},\ \ldots,\ J_z^{(FF)}(\phi_m)_{max} \right\} \quad . \tag{56}$$

Using the numbers in set A and B, one is ready to apply the method of extrapolation function to obtain an error estimation.

3.4 APPLICATION OF THE EXTRAPOLATION FUNCTION TECHNIQUE TO THE ABOVE PROBLEM

From (55) and (56), we construct the following extrapolation function $R_i(\omega)$,

$$R_i(\omega) = \frac{J_z^{(FF)}(\phi_i)_{max}}{J_z^{(ATH)}(\phi_i)_{max}} \quad . \tag{57}$$

From (57) we obtain an average function $F1(\omega)$ as follows:

$$F1(\omega) = \sqrt[N]{R_1(\omega)\ R_2(\omega)\ \ldots\ R_N(\omega)} \quad . \tag{58}$$

Then the following ratio $Q1_i(\omega)$ is calculated

$$\left| Q1_i(\omega) \right| = \left| \frac{R_i(\omega)}{F1(\omega)} \right| \quad . \tag{59}$$

In the examples given in Figures 23 and 24 only three angles of incidence are used, i.e., $\beta_k = \pi/4,\ 0,\ -\pi/4$, in calculating $J_z^{(ATH)}(\phi_i)_{max}$. On the other hand, incident waves with β_k which varied from $-\pi/2$ to $+\pi/2$, are used to calculate $J_z^{(FF)}(\phi_i)_{max}$. The function $|Q1_i(\omega)|$ is plotted as

a function fo frequency in Figure 23 for a cylinder with d ≈ 1 m, a = 0.5 m, R = -1. The variation is only a factor near 2.

In Figure 24 the same calculation is applied to the cylinder, however, with R_1 = -0.75 for an assumed imperfect ground reflection. The variation is a factor of 2.5 for eight positions. This is a better error bound as compared to those obtained for a single incident wave. However, these conclusions are obtained under the assumption that the maximum current density can be used in estimating the error.

REFERENCES

1. Stratton, J. A., Electromagnetic Theory, McGraw-Hill: New York, 1941, Chapters VI and IX.

2. Baum, C. E., "Extrapolation Techniques for Interpreting the Results of Tests in EMP Simulators in Terms of EMP Criteria," EMP Sensor and Simulation Note 222, AFWL, 20 March 1977.

3. Merewether, D. E., J. F. Prewitt and C. E. Baum, "Characterization of Errors in the Extrapolation of Data from an EMP Simulator to an EMP Criterion," EMP Sensor and Simulation Note 232, AFWL, 25 October 1977.

4. Lee, K. M., R. Holland and K. Kunz, Calculation of the Transient Currents Induced on an Aircraft by 3-D Finite Difference Method, Mission Research Corporation, AMRC-N-45, October 1976, presented at APS-URSI Symposium, Stanford University, CA, June 1977.

5. Taylor, C. D., K. T. Chen and T. T. Crow, An Improvement on Wire Modeling for Determining the EMP Interaction with Aircraft, Air Force Weapons Laboratory, AFWL-TR-74-217, May 1976.

6. Harrington, R. F., Time-Harmonic Electromagnetic Fields. McGraw-Hill: New York, 1961, pp. 232-238.

7. King, R. W. P. and T. T. Wu, The Scattering and Diffraction of Waves. Harvard University Press: Cambridge, Mass., 1959, Chapters 2 and 4.

8. Row, R. V., "Theoretical and Experimental Study of Electromagnetic Scattering by Two Identical Conducting Cylinders", Jo. Appl. Phys., 26, 6, pp. 666-675, June 1955.

9. King, R. W. P., The Theory of Linear Antenna: Harvard University Press. Cambridge, Massachusetts, 1956 (Chapter IV).

10. Kao, C. C., "Electromagnetic Scattering from a Finite Tubular Cylinder: Numerical Solutions", Radio Science, 5, 3, pp. 617-624 March 1970.

11. Sancer, M. I. and A. D. Varvatsis (Northrop Corporate Labs),"Calculation of the Induced Surface Current Density on a Perfectly Conducting Body of Revolution", EMP Interaction Note 101, Air Force Weapons Laboratory, April 1972.

12. Merewether, D. E.,"Transient Currents Induced on a Metallic Body of Revolution by an Electromagnetic Pulse", IEEE Trans. EMC, EMC-13, 2, pp. 41-44, May 1971.

REFERENCES (Continued)

13. Perala R. A.,"Integral Equation Solution for Induced Surface Currents on Bodies of Revolution", IEEE Trans. EMC, EMC-16, 3, pp. 172-177, August 1974.

14. Holland, R., THREDE: A Free-Field EMP Coupling and Scattering Code, AMRC-R-85, Mission Research Corporation, September 1976.

APPENDIX A

SUPPLEMENTAL RESULTS FOR THE PROBLEM IN SECTIONS 1.3 AND 1.4

In this appendix, additional data are presented which supplement those presented in Sections 1.3 and 1.4.

In Figure A-1, the ratios $|Q_1(\omega)|$ at the angle $\phi = 0°$, refl = -1.0, a = 0.5 m, d = 5 m are compared using numerical solution of equation (25) with N = 7 and two approximations. (The results using N = 7 differ less than 0.1% as compared to those using N = 6.)

In Figure A-2, the ratios $|Q_1(\omega)|$ at the angle $\phi = 0°$, relf = -1.0, a = 0.5 m and d = 5 m are compared using numerical solution of equation (25) with N = 4 and two approximations. Note that the deep nulls shown in previous approximations disappear. (The results using N = 4 differ less than 0.1% as compared to those using N = 3.)

In Figure A-3, the ratios $|Q_i(\omega)|$ at different angles ϕ_i are calculated using numerical solution of equation (25) with N = 7, refl = -1.0, a = 0.5 m and d = 1 m. Comparing with figure 5 of section 1.4, this shows an error bound smaller than previous results.

In Figure A-4, the ratios $|Q_i(\omega)|$ at different angles ϕ_i are calculated using numerical solution of equation (25) with N = 4, refl = -1.0, a = 0.5 m and d = 5 m. This also shows a smaller error bound than previous results. The deep nulls and peaks shown in Figure 6 of Section 1.4 disappear here.

In Figure A-5, the ratios $|Q_i(\omega)|$ at different angles ϕ_i are calculated using numerical solution of equation (25) with N = 7 and refl = -0.75 for the ground, a = 0.5 m, d = 1 m. Comparing with Figure 7 of Section 1.4, this also shows an error bound smaller than previous results.

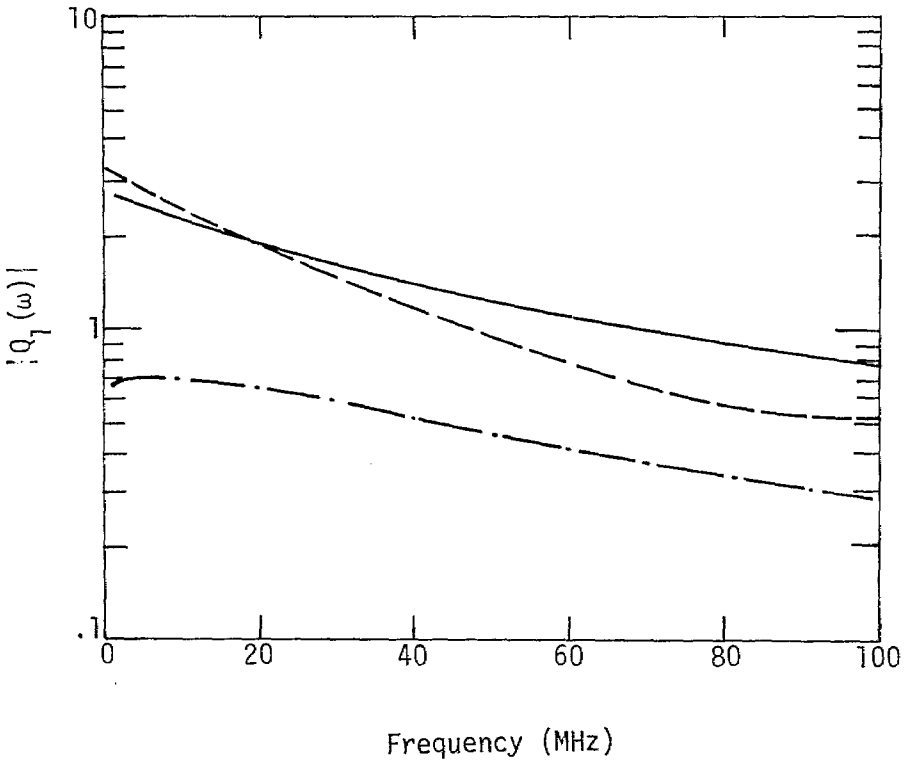

Figure A-1. The ratio $|Q_1(\omega)|$ at the angle $\phi = 0°$, reflection coefficient Refl = -1.0, a = 0.5 m, d = 1 m.

——— using numerical solution of Eq. (25) with N = 7
—·— using first approximate solution of Eq. (25)
– – – using second approximate solution of Eq. (25)

(cf. Figure 5, Section 1.4)

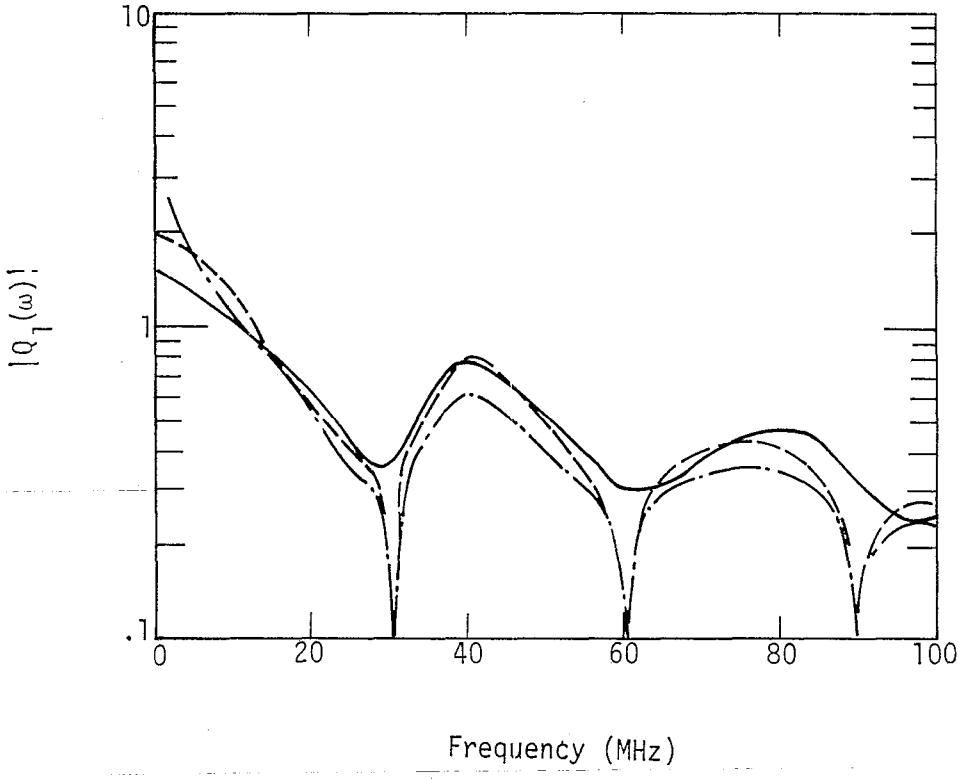

Figure A-2. The ratio $|Q_1(\omega)|$ at the angle $\phi = 0°$, reflection coefficient Refl = -1.0, a = 0.5 m, and d = 5 m.

——— using numerical solution of Eq. (25) with N = 4
—·— using first approximate solution of Eq. (25) (see Eq. (26))
— — — using second approximate solution of Eq. (25) (see Eq. (27))

(cf. Figure 6, Section 1.4)

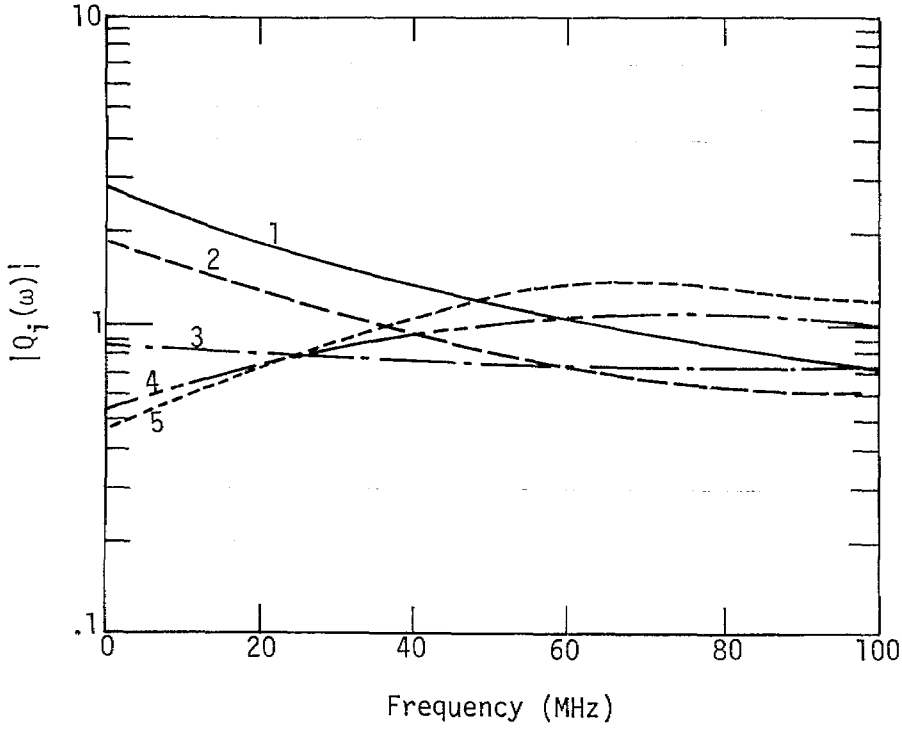

1 $\phi_1 = 0°$
2 $\phi_2 = 45°$
3 $\phi_3 = 90°$
4 $\phi_4 = 135°$
5 $\phi_5 = 180°$

Figure A-3. The ratio $|Q_i(\omega)|$ at different angle ϕ_i calculated using numerical solution of Eq. (25) with N = 7 and a reflection coefficient Refl = -1.0 for the ground, and a = 0.5 m, d = 1 m (cf, Figure 5, Section 1.4).

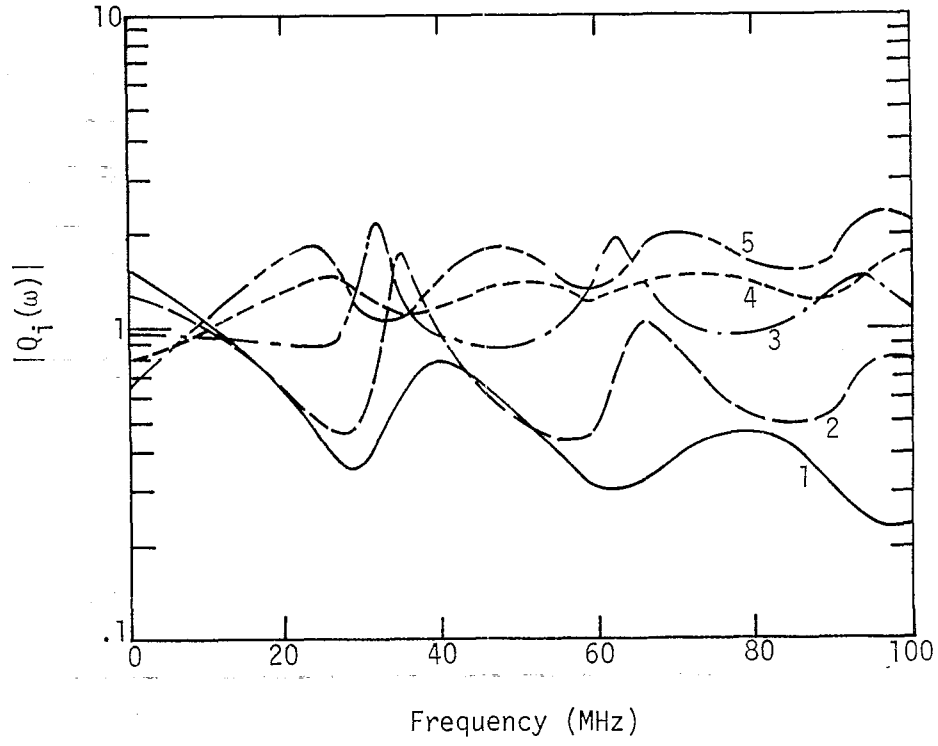

1 ϕ_1 = 0°
2 ϕ_2 = 45°
3 ϕ_3 = 90°
4 ϕ_4 = 135°
5 ϕ_5 = 180°

Figure A-4. The ratio $|Q_i(\omega)|$ calculated using numerical solution of Eq. (25) with N = 4 and a reflection coefficient of Refl = -1.0 for the ground, a = 0.5 m, d = 5m (cf., Figure 6, Section 1.4).

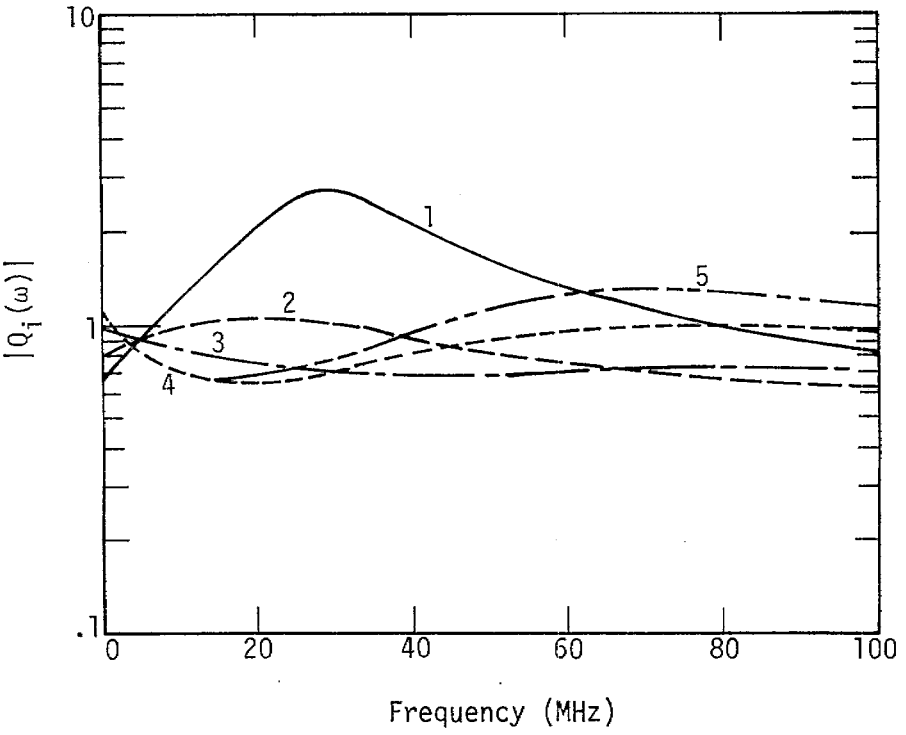

1 ϕ_1 = 0°
2 ϕ_2 = 45°
3 ϕ_3 = 90°
4 ϕ_4 = 135°
5 ϕ_5 = 180°

Figure A-5. The ratio $|Q_i(\omega)|$ at different angle ϕ_i calculated using numerical solution of Eq. (25) with N = 7 and a reflection coefficient Refl = -0.75 for the ground, a = 0.5 m, d = 1 m. (cf. Figure 7, Section 1.4).